Wireless sensing systems based on passive UHF RFID technology for physical parameters measurement

By

Shaheen Ahmad

A thesis submitted in partial fulfillment of the requirements for the degree of

Master of Science

In

Engineering management

Department of Mechanical Engineering

University of Alberta

Abstract

Sensing and monitoring using the conventional microwave, optical, and waveguide methods have been the focus of many researchers for the past two decades. However, the limitations imposed by these techniques such as power inefficiency and the use of complex readout circuitries are the important challenges for their successful implementation in the internet of things (IoT) based applications, when widespread deployment of sensors is essential. This dissertation focuses on the design of a new type of sensing systems utilizing a battery-less UHF RFID technology with the capability of power efficient remote sensing, reduced sensing node complexity, and lower maintenance over time.

Various capacitive interdigitated electrode (IDC) sensing elements were designed and evaluated for different sensing applications. The working principle is based on the capacitance variation of the sensing element due to the changes in the permittivity profile of the test medium that alter phase of the backscattered RFID signal. In order to use the high sensitivity advantages of the capacitive sensing element and the passive nature of the RFID technology; the designed IDC structures were integrated with a three-port RFID sensing architecture to develop a reliable non-contact passive remote sensing systems.

In the next step the proposed passive wireless sensing system was practically tested for remote liquid level detection in a real-world scenario. The presented solution is a simple three-port sensing architecture without any internal power source at the sensing node; that transduces liquid level variations into corresponding capacitance

change, that adds an additional phase delay to the input RFID signal. The phase variation of the backscattered signal is used to estimate the liquid level in real-time. Furthermore, this concept is expanded to the volume fraction analysis of a binary as well as multivariable mixtures by modifying the sensing element structure and utilizing the limited RFID frequency band while taking advantages of the multi-temperature measurements. The proposed method was evaluated by exposing the sensor to various mixtures containing different ratios of oil, alcohol and water. The difference in the phase values of the backscattered signal observed as a result of measurements at a single frequency (927 MHz) and multi-temperatures is used to calculate the unknown volume concentrations of the three components in a mixture based on the unique permittivity profile of the test samples. The presented sensing techniques provide a new solution for powerless real-time remote measurement in a densely populated sensing environment.

Preface

This thesis is an original work by Shaheen Ahmad submitted to fulfil the partial requirements of the master's degree in engineering management. The work is focused on the development of a new wireless sensing systems based on a passive wireless RFID technology.

Chapter 3 has been published as S. Ahmad, N. Khalid and R. Mirzavand, "Detection of Soil Moisture, Humidity, and Liquid Level Using CPW-Based Interdigital Capacitive Sensor," in IEEE Sensors Journal, vol. 22, no. 11, pp. 10338-10345, 1 June1, 2022, doi: 10.1109/JSEN.2022.3167337.

Chapter 4 has been published as Ahmad S, Khosravi R, Iyer AK, Mirzavand R. "Wireless Capacitive Liquid-Level Detection Sensor Based on Zero-Power RFID-Sensing Architecture," *Sensors*. 2023; 23(1):209. https://doi.org/10.3390/s23010209.

Chapter 5 will be submitted as S. Ahmad, R. Khosravi, A. Iyer, R. Mirzavand, "Volumetric characterization of multivariable mixtures using RFID based passive wireless capacitive sensor," in IEEE transactions on industrial electronics journal.

In all the publications Shaheen Ahmad is the main student contributor, he is responsible for the design, fabrication, tests, measurement, data collection as well as the manuscript composition. Prof. Rashid Mirzavand and Prof. Ashwin K. Iyer were the supervisory authors and involved in the concept formation and manuscript edits.

Acknowledgment

I would like to take this opportunity to express my gratitude and sincere thanks to my supervisor Prof. Rashid Mirzavand and my co-supervisor Prof. Ashwin K. Iyer for their guidance, valuable thoughts, and continued support throughout my research and study at the University of Alberta. I would also like to thank Dr. Ramin Khosravi for his guidance and support during my research that helped smooth and successful completion of this project. I'm also grateful to Prof. Kambiz Moez for his insightful comments and for serving as an examiner to evaluate this research work.

A special thanks to my colleague Nabil Khalid for his research collaboration and valuable insights at the start of my research project. I am also thankful to him for sharing his PhD research materials to collaborate and further extend the research directions based on his previously developed work as a result of his PhD research at the University of Alberta.

My appreciation extends to all my group members for their collaborative attitude and insightful contribution. I always appreciate the constructive discussion with all my colleagues that helped us improve our knowledge and experience.

My deepest gratitude and thanks to my family members for their support and encouragement throughout my life in every situation. They always mentored me and offered their help at every stage of my academic career.

I gratefully acknowledge the financial support from NSERC, and Future energy systems for providing financial support, and CMC Microsystems for providing simulation tools that helped accomplish the project objectives.

Table of Contents

List of Tables

List of figures

List of Acronyms

RFID	Radio Frequency Identification
IDC	Interdigitated Electrode Capacitor
MUT	Material Under Test
RF	Radio Frequency
TDR	Time Domain Reflectometry
GCPW	Grounded Co-Planar Waveguide
IoT	Internet Of Things
VNA	Vector Network Analyzer
IQ	In-phase and Quadrature
HFSS	High Frequency Structural Simulator
RH	Relative Humidity
UHF	Ultra-High Frequency
ADS	Advanced Design System
MAE	Mean Absolute Error

Chapter 1 Introduction

1.1. Motivation

The advancement in modern communication technologies requires widespread deployment of sensing systems to monitor and control environmental physical parameters. Real-time data acquisition using densely populated wireless sensing nodes is the demand for the current and new internet of things (IoT) applications. Owing to its demand, remote sensing has achieved a great deal during the last few decades with their applications in many modern industries such as oil and gas, smart agriculture, food production, chemical, biomedical and so on. However, new more reliable and energy efficient sensing methods need to be developed to wirelessly monitor the environmental variables in real-time with reduced power consumption, design cost, and maintenance.

The conventional microwave, waveguide, and optical methods are among the main sensing techniques due to their unique sensing capabilities; however, they utilize complex signal processing circuits to convert the sensed data to a measurable information and then send it wirelessly. These sensors utilize internal power source to drive the complex circuits that increase cost and require regular maintenance over time, making them impractical for many applications. The energy consumption and high design and maintenance cost cannot be ignored for applications where widespread deployment of sensing nodes is essential.

RFID based wireless sensors due to their passive nature, design simplicity, high reliability, the ability to non-contact sensing and the elimination of the internal power

source have achieved great success during the last decade [1][2]. RFID based wireless sensing nodes harvest energy from the signal sent by the reading device, thus provide design simplicity and increased reliability. However, to utilize the advantages of the RFID systems, the conventional tag design needs to be engineered to develop new sensing nodes based on the type of targeted applications [3-5]. Thus, energy efficient and more reliable sensing systems can be developed by utilizing the zero-power RFID systems without compromising much on the sensing capability and the wireless read range.

1.2. Objectives

The main objective of this thesis is to develop a reliable battery-less RFID based monitoring systems for remote measurement of the environmental parameters with a focus on reducing power consumption, cost, and complexity of the sensing nodes while still preserving the sensor's sensitivity and a reasonable read-range. To achieve this goal, several sensing systems targeting specific applications were developed using passive RFID architecture and a capacitive sensing elements for a battery-less remote sensing of environmental parameters.

- The feasibility of the interdigitated electrode capacitor (IDC) based sensing element is evaluated for the moisture content detection in both air and soil by taking advantage of the variation in the IDC capacitance due to changes in the permittivity of the test medium surrounding the capacitor.
- Part of this thesis is devoted to the design and analysis of a passive wireless sensing system for remote liquid level detection using RFID based sensing

architecture. The new sensing system has the capability to detect and estimate the liquid height remotely with a good sensitivity and without the use of any complex readout circuitry by utilizing the phase variation of the sensor as a sensing parameter.

- Apply the advantages of a battery-less RFID systems to the remote volume fraction measurement of a multivariable mixture in real-time using phase measurements in a limited frequency bandwidth while taking the advantages of a multi-temperature measurement to obtain multiple sensing information with the application focusing on the oil and gas industry.

The proposed sensing systems offer simple, more reliable, and energy efficient sensing solution, that could be the start of a new generation of wireless sensing devices.

1.3. Thesis Outline

The thesis is divided into six main chapters and is written in a paper-based format.

Chapter 1, introduces the motivation and research objective of this work.

In chapter 2, a literature survey and background on sensors developed for physical parameter sensing is discussed. First, several RF/Microwave and other sensing techniques are presented with their advantages and limitations for water content detection in soil as well as in the air. Sensors used in the literature for the level detection of various types of liquid are also discussed and categorized based on their working principle. Followed by the review of sensing techniques developed for the volume concentration measurement of a binary and multivariable mixtures.

Chapter 3, discuss the design of an interdigitated electrodes capacitive sensing element for the detection of soil moisture and air humidity. The sensor was practically tested based on the principle of the phase variation at a fixed frequency caused by the change in the capacitance due to the difference in the water content concentration of the test medium. The proposed sensing element demonstrates a good sensitivity to the water concentration detection in a soil as well as air.

Chapter 4, introduces the design of an RFID based wireless sensing architecture that integrates a capacitive IDC sensor for the liquid level detection in real-time. The capacitive sensing element is designed to have a resonance at the operation frequency that changes with the liquid level variation altering the phase of the input signal with high sensitivity. Thus, the change in the liquid level is translated to the phase variation of the input backscattered signal, which is detected at a wireless RFID reader. The proposed method offers a more reliable technique for passive wireless detection of liquid level in real-time.

In chapter 5, a new method for the volume fraction measurement of a multivariable mixtures containing three materials with unknown concentration is proposed and investigated. The sensing system comprises of a capacitive sensing element and a power-less RFID sensing architecture. The capacitance of the sensing element is affected by the changes in the real permittivity profile of the test samples that alters phase of the input signal received from the RFID reader. By performing phase measurement of each sample at a fixed frequency and two temperatures, a set of three linear equations can be obtained. The unknown volume fraction of the material in a

mixture can be calculated by solving the linear system of equation. The sensor performance is analyzed for both binary and multivariable solutions, offering a high accuracy with the capability of real-time wireless sensing and design simplicity.

Finally, the conclusion of the thesis is provided in chapter 6, with some insights about the future work.

Chapter 2 Background

This chapter presents a literature review on different sensing techniques for the detection and monitoring of various environmental physical parameters. A range of sensing techniques such as impedance spectroscopy, resistive and capacitive methods for moisture content detection of a medium is reviewed. Liquid level detection sensors are also classified based on their operation principle and design complexity. The final section focuses on the investigation of sensors for material characterization and volume fraction measurement of a binary and multivariable mixtures. Resonance and optical based sensors are discussed and finally RFID based sensing systems are presented as a competing sensing technique.

2.1. Sensing techniques for water/moisture content measurement

Various sensing methods have been developed for water/moisture content measurement in a medium under test. Although, the measurement techniques are different, the working principle is based on observing changes in a measurable variable that directly relates to water content variation of a medium; such as permittivity, conductivity, capacitance or resistance. Water is a high permittivity substance with a dielectric constant value of 80 (at 20^{o}C) [6]. Therefore, the sample permittivity increases with the amount of water content, thus, dielectric measurement techniques have been very popular for moisture content measurement. Time-domain reflectometry (TDR) is a traditional technique for permittivity measurement based on the time required for an electromagnetic signal to travel along the line surrounded by a test medium. Moisture content measurement using TDR is studied in [7]. Two

parallel probes were used to detect moisture in soil media by measuring their resistance as shown in Fig. 2.1. It was revealed that good accuracy could be obtained for sandy and loamy soil, however, the sensor accuracy decreases significantly when moisture content exceeds 30% in clay soils. It should be noted that TDR techniques are based on very precise measurements for accurate wave interpretation that require complex electronics that limit their use for many applications.

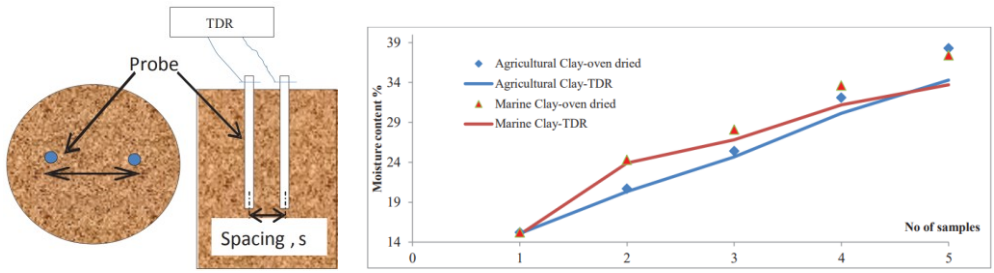

(a) (b)

Figure 2.1. (a) Sensor schematic diagram from top and side view (b) Discrepancy in moisture content determination of the proposed sensor in two clay samples [7].

Measurement using dielectric resonators is another popular technique for detecting water content in a medium. The resonance frequency of a dielectric resonator is a function of the permittivity of a medium which changes with the dielectric constant. The resonance structure may be a ring resonator [8], a complementary split-ring resonator [9], a microstrip resonance ring [10], and so on. Fig. 2.2 shows the schematic diagram and the fabricated prototype of a microstrip resonator ring for soil moisture detection. The variation in the resonance frequency with respect to the dielectric constant and the complex permittivity change with respect to water content is also given in Fig. 2.3 (a) and (b) respectively. Impedance spectroscopy is also used

to determine the amount of water concentration in the soil/air as well as the concentration of other minerals and ions. In [11] a multi-frequency impedance measurement approach is used to estimate the moisture and ionic concentration in soil by using dielectric mixing models. In spite of the fact that this technique can provide a reasonably accurate estimate, the use of multiple frequencies at multiple concentration levels and dielectric mixing models such as debye-type dielectric relaxation makes the measurement considerably more complex. Furthermore, according to [12], dielectric mixing models are not effective at high RF frequencies (over 100 MHz).

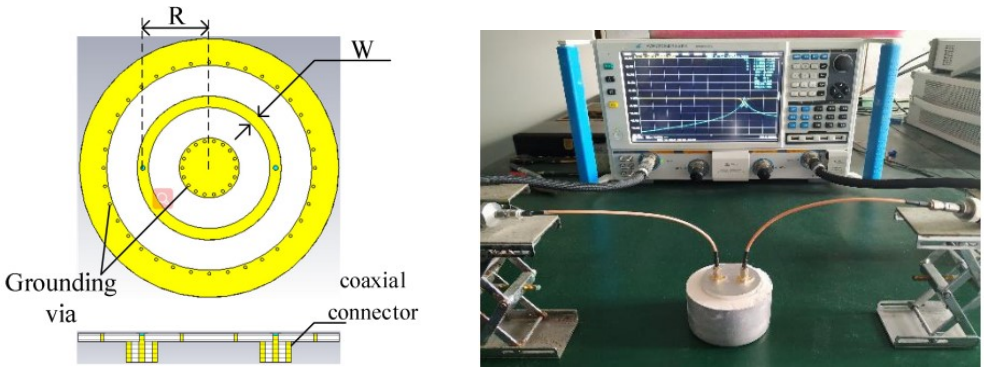

(a) (b)

Figure 2.2. (a) Top and profile view of MRR sensor. (b) Experimental measurement of the MRR sensor [10].

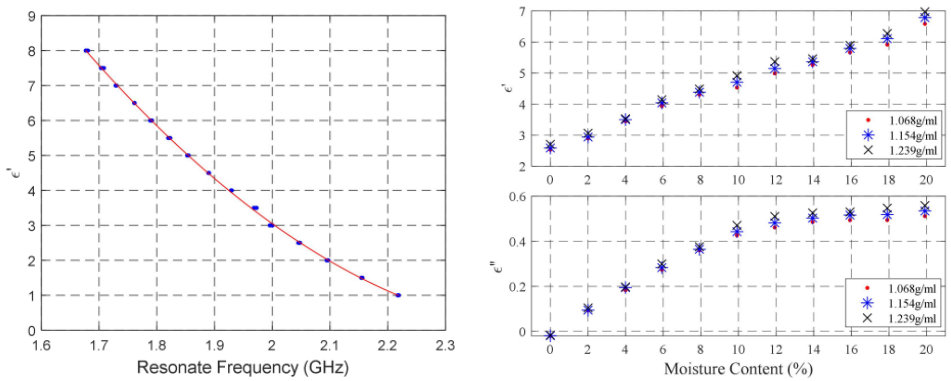

Figure 2.3. (a) Fitting curve between the real part of the dielectric constant and resonant frequency (b) Measured results for dielectric constant versus moisture content variation from 0% to 20% [10].

Humidity and soil moisture measurements are carried out using either resistive or capacitive sensing techniques. Since resistive sensors work based on electrical conductivity, at a low moisture content and humidity level the conductivity is very poor which makes the sensor unable to respond [13]. In addition, resistive sensors are inefficient because their resistance increases with dielectric constant. Therefore, capacitive sensors, based on their energy efficiency and sensitivity to the change in relative permittivity, are preferred. Capacitive sensors provide a stable, linear, and fast response to a wide range of variations in dielectric constant. Capacitive sensing based on an interdigital capacitor has been widely exploited during the past decade [13]-[17]. However, in case of humidity monitoring, these sensors require an additional sensing layer for better sensitivity. An IDC based capacitive sensor is designed for humidity measurements as shown in Fig. 2.4. using Gallium nitride (GaN) as a sensing layer. The sensor offers improved sensitivity and efficiency to the humidity variation for a wide range of 0 to 100% humidity, as well as good capacitance stability as demonstrated in Fig. 2.5. Researchers have studied a variety

of sensing materials, including organics [18], polymers [19], oxides [20], and biodegradables [21] to enhance humidity sensor performance for diverse applications. Some authors are working on the combination of materials for the sensing layer, although polyamide-based sensors are among the most commonly reported for humidity sensing.

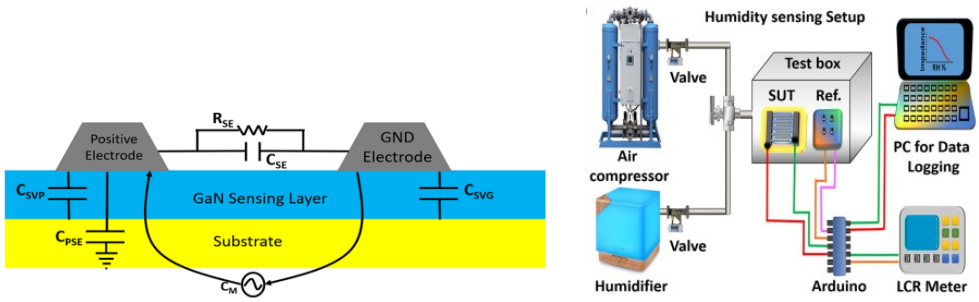

(a) (b)

Figure 2.4. (a) Schematic diagram of the sensor (b) Measurement setup for humidity sensing [12].

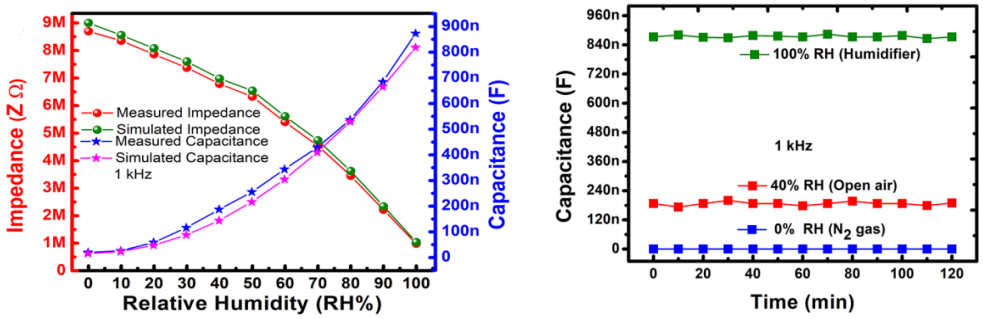

(a) (b)

Figure 2.5. (a) Measured and simulated impedance and capacitance response of the sensor at 1 kHz. (b) capacitance stability plot [12].

2.2. Overview of liquid level detection sensors

Wireless liquid level detection is essential due to its practical use in many real-life applications, including smart homes, healthcare, petroleum, food and agriculture.

Detection of liquid level is divided broadly into few categories such as classification based on the type of measurement, i.e. continuous level measurement [22] for process monitoring or point level measurement [23] for marking a single liquid level height to activate an alarm. These sensors are further classified based on their contact [24] and non-contact [25] nature with the sensing medium. The accuracy of contact type sensors is usually smaller due to their dependence on liquid properties that affect the sensor performance, mostly in the case of conducting type liquids; therefore, non-contact level measurement is widely explored in the literature. Although most of the work is focused on the sensitivity and detection range improvement, much less emphasis has been given to the development of low power reliable sensing nodes that can be densely deployed for applications such as wireless IOT. Most of the liquid detection sensors need a wired connection or a built-in battery to operate, that increases design complexity, cost and require regular maintenance making them unsuitable for many modern sensing applications [26].

Several liquid level detection sensors have been presented in the past based on multiple design techniques. Coaxial cylindrical probe sensors are widely known level sensors having a reasonable accuracy and linearity, but they are bulky and require a high amount of power to operate [27]. A grounded cylindrical coaxial sensor for conductive liquid level measurement is shown in Fig. 2.6. having very linear capacitance response with respect to liquid level. Although the capacitance needs to be converted to a measurable quantity using signal processing circuits to detect the liquid level. Additionally, these sensors are bulky in size.

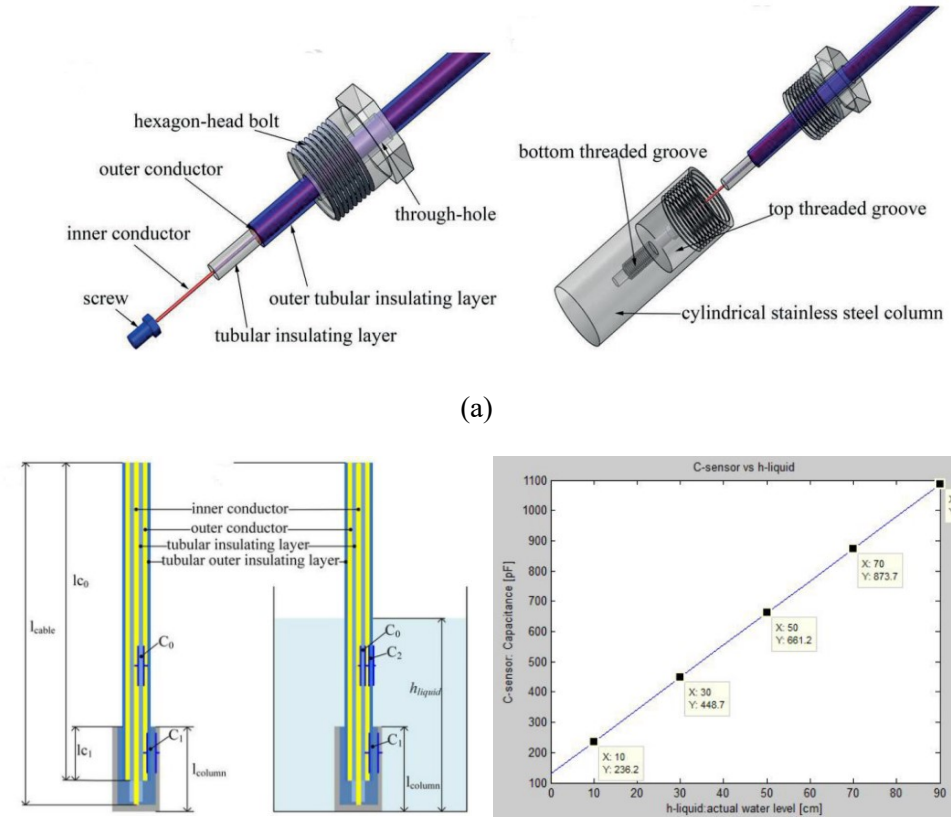

Figure 2.6. (a) Schematic of the cylindrical capacitive sensor. (b) Analysis of the sensor in liquid. (c) Sensor capacitance response versus liquid height [27].

Optical [28] and ultrasound [29] sensing techniques provide high resolution liquid level measurement; however, the optical technique has high manufacturing and maintenance cost as well as health and safety issues while the ultrasound measurement is mostly erroneous due to its sensitivity to environmental conditions. Microwave resonators [30], acoustic wave resonators [31], interdigitated electrodes [32] and comb electrodes [33] are other popular techniques for liquid level measurement, however, they utilize complex digital circuits for signal processing that require additional power to operate resulting in lower power efficiency, increased

cost and design complexity. An example of a power inefficient and bulky liquid level sensor is given in Fig. 2.7. which is based on interdigitated electrode capacitor connected to a digital circuitry to detect and display the liquid level height. In order to perform accurately these sensors, require a reference electrode structure for proper calibration.

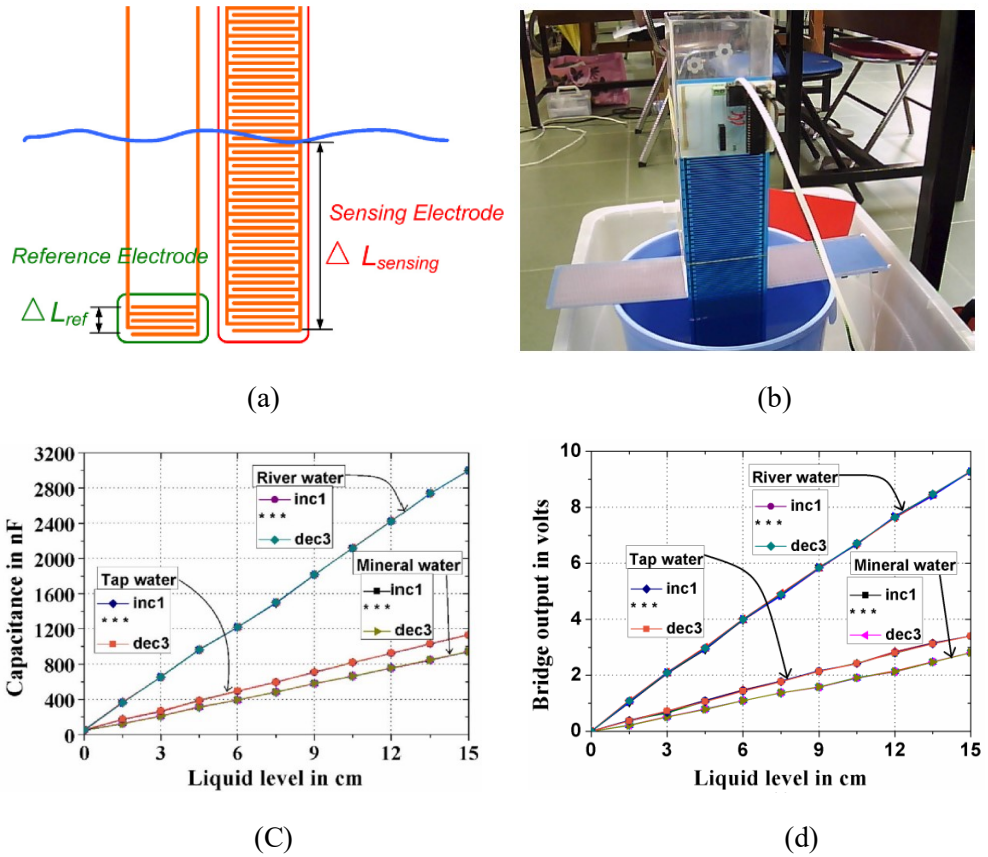

Figure 2.7 (a) Sensor design and arrangement for liquid measurement (b) Experimental setup for liquid detection (c) capacitance curve of the sensor for different liquids (d) output voltage curve for different liquids [32].

Recently, some efforts were made to use RFID technology for liquid level detection. A wideband frequency measurement using a chipless sensor is performed, as shown

in Fig. 2.8; however, the obtained results are non-linear for different liquid levels. Additionally, a very short wireless detection range of below 50 cm is possible based on the proposed sensing system [34]. Several other RFID based sensors have been developed that can detect liquid within the container, but lacks the capability of providing continuous information on the liquid level variation in real-time [35-37]. Fig. 2.9. shows an RFID tag enabled container that reports whether the container is filled with liquid or is empty based on the received backscattered power by the RFID reader. Sensing systems based on semi-passive RFID technology has been the focus of many researchers [38-40], due to their higher read-range as compared to the passive RFID systems. Despite they use signal from the reader to energize the chip, semi-passive RFID technology also require an internal power source to drive the electronic circuits, making them unreliable, bulky and costly. Some other type of battery-less RFID systems available in the market incorporates digital circuitry that can add the sensed information digitally to the backscattered signal with better accuracy and with the capability to integrate off-the-shelf sensors, however, the power required by the digital circuits highly reduce the sensing read-range [41[42]. In [43] a passive RFID chip-based design is presented with a read range of up to 7.5 meters, although, it can only be used as a flood sensor without providing any information about the liquid level height. Therefore, Further design investigation of the RFID based sensors is needed to develop sensing nodes that can fulfil the current and future wireless sensing requirements.

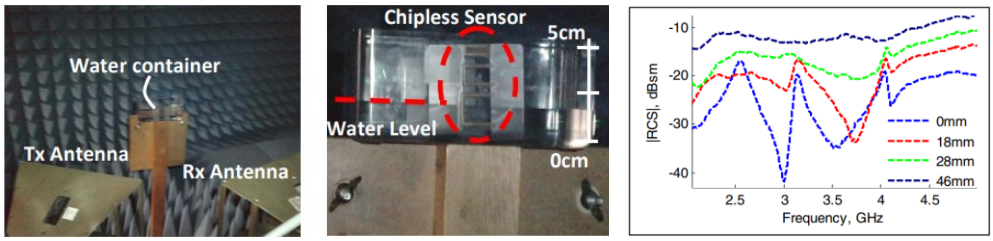

(a) (b)

Figure 2.8. (a) Measurement setup for chipless RFID level sensor. (b) frequency domain results for different liquid levels [34].

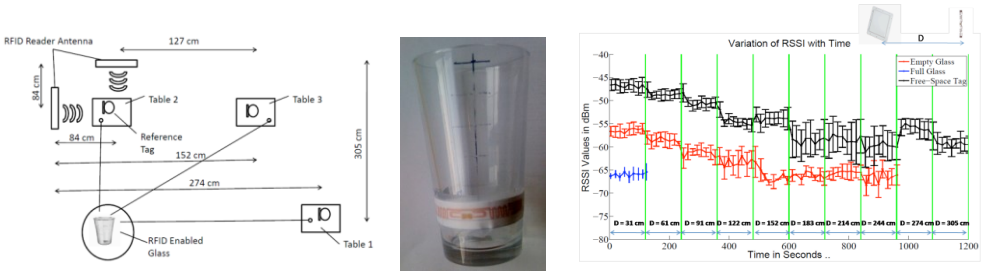

(a) (b) (c)

Figure 2.9. (a) Measurement environment setup. (b) Proposed RFID tag enabled container (c) measured response of the sensor for various range distances [35].

2.3. Sensing methods for material characterization and volume fraction calculation of a mixture

There has been a lot of interest recently in the literature for developing different sensing methods that can estimate volume fractions in a binary and multivariable liquid. Among these methods, microwave sensors are the most widely used dielectric characterization sensors that are mainly classified into two categories. The resonance sensors [44][45] and the transmission line sensors [46-48]. Microwave resonance sensors utilize shift in the resonance and its quality factor at a fixed discrete frequency point to characterize materials, therefore, providing a limited number of sensing

parameters that limited their applications to the sensing of binary samples only. Transmission line sensors, however, provide relatively more sensing information based on the broadband measurement of transmission and/or reflection coefficients over a given frequency range. Fig. 2.10. shows a split ring resonator (SRR) based sensor that can estimate the volume percentage of a multivariable mixture using a broadband transmission response. Different transmission response can be observed from the measured results by loading the sensor with different materials. Although, almost all of the previously reported broadband transmission line sensors are designed for low volume sensing, providing sensing information about the sample that are either injected into the microfluidic channel/test tube [49] or placed on a sensing element, in addition they are limited to the use of specific frequency bands [50]. Coaxial probe sensing is a popular dielectric characterization method that has gained a lot of interest in the past [51]. The drawback of these sensors is their non-planar structure that increases design complexity and hence associated with high cost. Additionally, a specific amount of sample volume is required for submerging the probe that reduce the measurement accuracy for many applications [52].

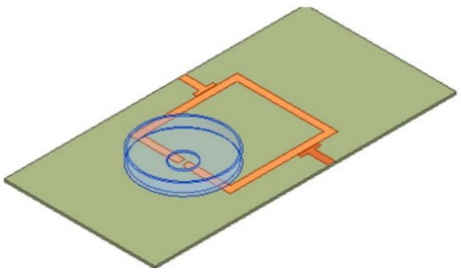

(a)

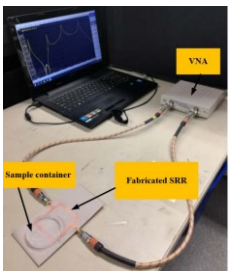

(b)

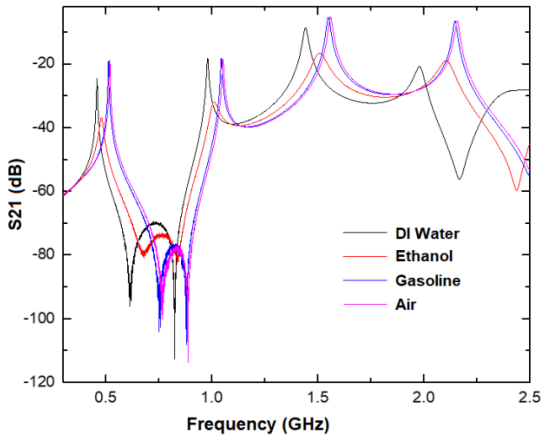

(c)

Figure 2.10. (a) Perspective view of the SRR sensor. (b) Experimental setup for multivariable mixture analysis. (c) Transmission response of the sensor for different materials [41].

Amongst other non-intrusive techniques, optical sensing is largely investigated, but they are not suitable for certain industrial applications as they rely on the use of optically-transparent solutions as well as other limitations such as high design and maintenance cost [53]. The radiographic solutions such as X-rays and gamma rays provide reasonably high sensing accuracy, however, these radiations are harmful for human body [54]. The non-contact capacitive sensing technique provide some additional advantages over the other solutions such as design simplicity, robust sensing capability and low cost which makes them more popular for a wide range of sensing applications [56-57]. A cross capacitance-based sensor for material characterization and detection of moisture level in oil is proposed as shown in Fig. 2.11. The sensor works based on the difference in the permittivity values of the test components. Although, the volume fraction measurement capability is not analysed,

the sensor works well for characterizing and detecting various types of Oil samples as well as the moisture concentration within the samples.

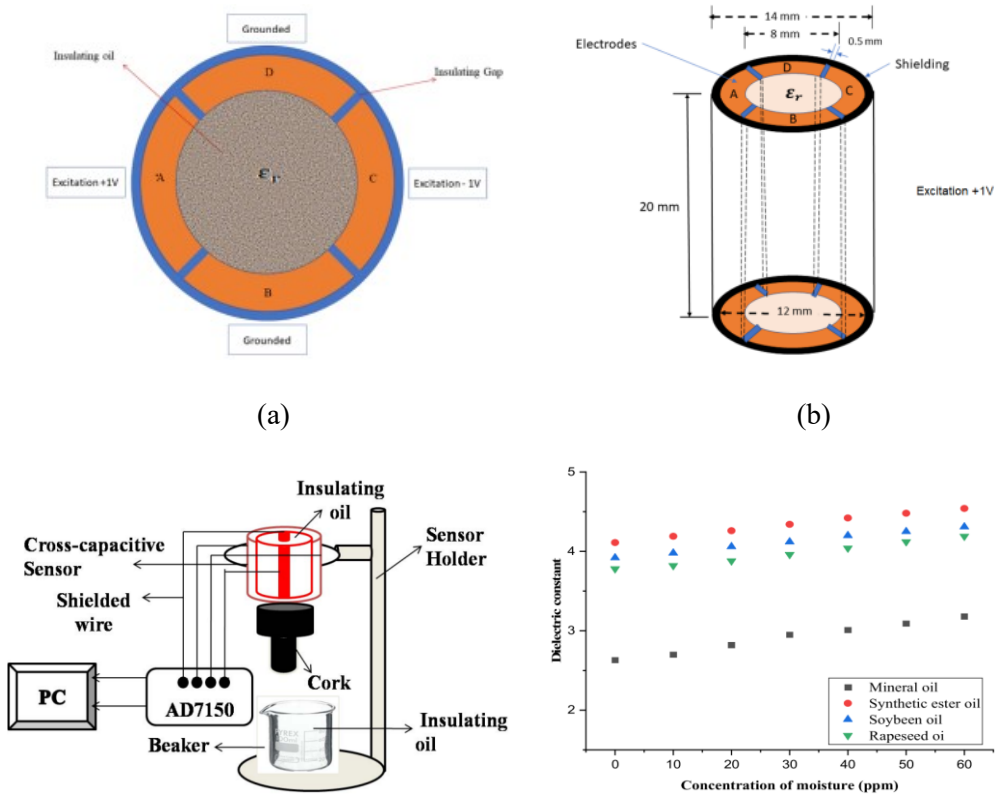

Figure 2.11. (a) Top view of the proposed sensor (b) Schematic of the sensor. (c) experimental setup for material characterization. (d) Dielectric constant of different liquids with different moisture concentrations [51].

RFID based sensors have recently gained a lot of interest, due to their advantages such as reduced maintenance and lower overall cost by eliminating an internal power source, unlike typical sensors that require periodic maintenance, which is a problem if the sensor is installed in a harsh environment and/or is hardly accessible [58]. Apart from their use in the supply chain industry, RFID sensors have been used as a low-cost solution for temperature monitoring [59], flow sensing [60], pressure monitoring

[61], gas sensing [62] and so on. RFID technology is also being used as a material characterization and volume concentration measurement systems, however, they are facing some challenges that need to be addressed. In [63], a passive UHF RFID chip-based sensor is used for ethanol concentration measurement in water from 25% to 100% ethanol concentration, however, the sensing method is limited to the detection of binary liquid mixtures only, as well as the read-range is below 1 meter. Another passive RFID sensor for a binary liquid concentration measurement is designed utilizing a wide frequency band with a reasonable read-range of up to 5.8 m [64]. Chipless RFID sensors are also evaluated due to their design simplicity and power efficiency by eliminating the integrated circuits (IC) from the tag and utilizing variation in radar-cross-section (RCS) for sensing, although they also suffer from the same limitations of short read-range and limited detection capability [65-67]. Power efficient battery-less RFID sensors are used as a material characterization sensor for a wide range of applications that harvest energy from the RFID readers or NFC devices to drive the electronic circuitry [68-70]. The digitization circuitry used in these types of sensors, digitally add the sensed parameters to the backscattered RFID signal with improved accuracy, however, the extra power required by the digital circuits reduces the read-range as well as due to the limited sensed information they are mostly limited to the detection of binary mixtures only.

Chapter 3 Detection of soil moisture and humidity using GCPW based interdigitated electrodes sensor

The limitations of the water content measurement sensors highlighted in chapter 2 can be improved by designing more efficient sensing elements. This chapter presents the design of a highly reliable, energy-efficient, ultra-high frequency (UHF) capacitive sensing element that can measure the moisture and humidity level of a test medium. The principle of sensing is based on a reactive phase variation of the input signal upon reflection, whereas its amplitude and phase are actively changing with variations in the dielectric constant of the test medium. This new sensing element provides high reliability, good sensitivity, low power consumption, and can be implemented in a number of applications, including agriculture, oil and gas industry, land and water treatment, medical equipment, and biotechnology.

3.1. Theory

3.1.1. Sensor Design Using IDC

Interdigital capacitive sensors have been extensively used for the estimation of material dielectric properties due to their simplicity, high sensitivity, and low cost. The IDC is composed of interdigital electrodes that can be fabricated using conventional metal grids on the PCB. The working principle of the IDC sensor is based on the change in its reactive capacitance as a function of change in the dielectric properties upon penetration of the fringing electric fields into the test medium (MUT). A novel IDC sensor is designed in this work by integrating the coplanar waveguide (CPW) feeding with the interdigitated capacitor as depicted in Fig. 3.1 (a). The power

flow is only contained within the feedline and the capacitor, making the IDC sensitive to the dielectric change while the rest of the structure is insensitive. This improves the accuracy of the measurements by reducing uncertainties in the results. Fig. 3.1 (b) demonstrates that the maximum current density occurs only in IDC structures and feedlines. The sensor is designed on a Rogers RO4003 substrate (ε_r= 3.55) with the IDC dimensions of 24mm × 40mm and overall dimensions of 80mm × 57mm × 1.6mm. Sensor dimensions, including electrode length and width, electrode gap, and electrode number, have been optimized to improve sensor performance. Unlike parallel plate capacitors, the analytical equation for calculating the capacitance of the IDC is more complex and depends on the substrate material, the IDC dimensions, and properties of the test medium. The capacitance expression was first proposed by Olthuis et al. [71], which was further studied and reported by several authors [72], [73]. The capacitance formula for the interdigital capacitive sensor is given by [72],

$$C = L(N-1)\left(\frac{\varepsilon_0\varepsilon_{r,t}}{2}\frac{K\sqrt{1-k^2}}{K(k)} + 2\varepsilon_0\varepsilon_{r,m}\frac{h}{d}\right) \quad \text{……. (3-1).}$$

where, L is the length of the electrodes, N is the number of electrodes, ε_0 is the permittivity of vacuum 8.854 × 10−12 F/m, $\varepsilon_{r,m}$ is the permittivity of the test material, h and w are the thickness and width of the electrodes respectively, d is the spacing between the electrodes and $K(k)$ is the first order elliptical integral to calculate the impact of fringing fields, where k can be represented by,

$$K = Cos\left(\frac{\pi}{2}\frac{w}{d+w}\right) \quad \text{…….. (3-2).}$$

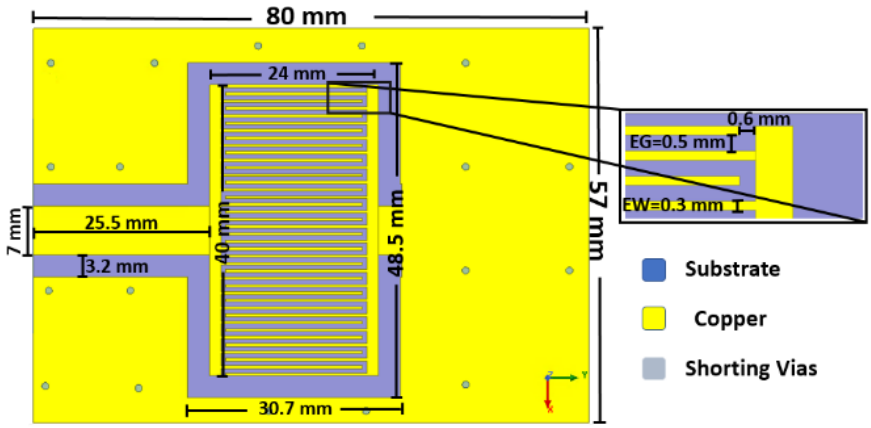

(a)

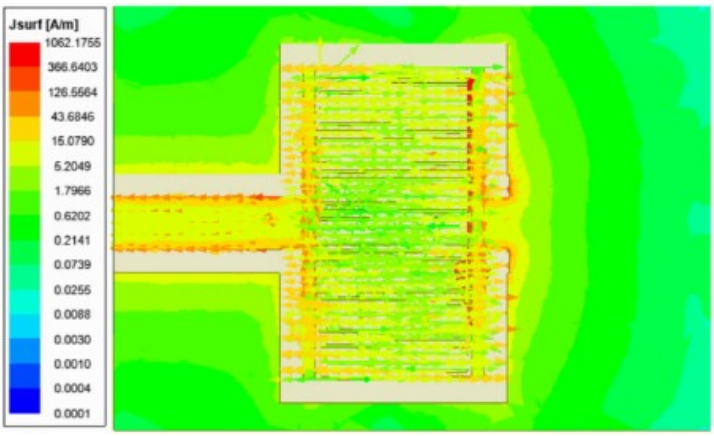

(b)

Figure 3.1. (a) Proposed design of interdigital capacitive sensor. (b) Surface current density.

3.1.2. Working Principle

The simplest model of the interdigitated electrode capacitor connected to a transmission line can be represented by Fig 3.3. The characteristic impedance of the transmission line is represented by Z_o which is designed to have an impedance of 50 Ω. The impedance of the load capacitor is denoted by Z_c. The load reflection coefficient can be represented by the expression given below,

$$\Gamma_L = \frac{Z_c - Z_o}{Z_c + Z_o} \quad \text{..... (3-3)}$$

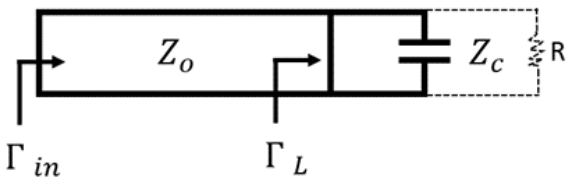

Fig 3.2. Simplified representation of a capacitive load connected to a transmission line.

From 3-3, the reflection from the load will be smaller if the load impedance value is equal or close to the characteristic impedance value. According to our requirements we keep the response of the IDC to behave as a capacitive load, therefore the load impedance is not equal or close to the characteristic impedance value ($Z_o = 50$), thereby most of the incident power is reflected back from the load. The reflected signal, however, undergoes a phase transition due to the variation in the IDC capacitance as the permittivity of the surrounding changes. The angle of the reflected signal can be represented by 3-4. From the equation, θ_{sensor} is the phase delay caused due to change in the capacitance of the IDC with respect to variation in the material under test. This phase variation of the reflected signal is used as a sensing parameter for the detection of water content as well as the detection of other environmental parameters reported in the subsequent chapters of this research work.

$$\Gamma_L = e^{j\theta_{sensor}} \quad \text{..... (3-4)}$$

However, capacitance of the load capacitor is not the only parameter that is changing. In case of water detection, the complex part of the dielectric constant introduces a resistive factor that can be represented as a parallel connection to the capacitance part

as shown in Fig 3.3. Although in our developed IDC sensing elements, we optimized the structure dimensions in a way to have very small change in the resistance as compared to the capacitance when the permittivity of the MUT is varied. Therefore, we consider that the effect of the resistance on the measurement is not very significant and can be ignored for the proposed sensing elements.

3.1.3. Sensitivity and Sensing Layer Characteristics

The sensing layer is an important part of the design. The type and thickness of the sensing layer is a key factor affecting the sensor's capacitance, sensitivity, and penetration depth. The sensor capacitance is greatly affected by the electric field penetration depth into the sensing layer and the test medium. Therefore, it is important to determine the penetration depth of the fringing fields originating from the electrodes to evaluate the sensor performance. However, there is no clear definition of the electric field penetration depth in the literature because it is almost impossible to determine its actual value. Some authors suggested that the effective penetration depth is the value when the sensor's terminal impedance equals to 3% of the difference between the minimum and maximum value of the terminal impedance [74]. In [75] a mathematical expression for the distance of the penetration depth is used as one third of the electrode's width (E_w) plus the gap between the electrodes (E_G), represented by (3-5). These two parameters are shown in Fig. 3.1 (a). According to the given equation, the electric field penetration depth is approximately 305 μm according to our proposed dimensions.

$$PD = \left(\frac{E_W + E_G}{3}\right) \quad \ldots\ldots\ldots (3\text{-}5)$$

The sensor is simulated using two layers on top of the sensor, the first layer is a sensing layer (PVA) and the second layer is a test medium (Soil or Air). At first the PVA layer thickness is considered to be roughly equal to the penetration depth (305 μm), therefore 100% of the electric fields were contained within the first layer and the capacitance and phase change is only due to the permittivity change in the sensing layer. In the second case the sensing layer thickness has been reduced to half the electric field penetration depth. In this case, the effect on the sensor's performance is due to a change in the permittivity of both the sensitive layer as well as the test medium. By further reducing the sensing layer thickness (to 20% of the electric field penetration depth) the electric fields are mostly contained within the test medium and therefore the variation in the capacitance and phase is mainly due to the permittivity change within the test medium. From Fig. 3.2 (a) the S11 phase variation is larger for the thinner (60 μm) sensing layer as compared to the thicker (305 μm) layer. The reason for this is the higher permittivity change due to the presence of more water content in the test medium than in the sensing layer. This is only true for the simulation results up to 60% relative humidity. In the case of experimental results above 60%RH, the phase variation increases with the increase in the sensing layer thickness. The phase variation and sensitivity (Fig. 3.2) are plotted against change in the water content between 10% (r = 4) and 60% (r = 52).

Generally, the sensitivity of the IDC sensing element is represented as the ratio between the capacitance variation and the variation in the relative dielectric constant [76,80], denoted by,

$$S_{\frac{\delta C}{\delta \varepsilon}} = \left(\frac{C_m - C_0}{\varepsilon_m - \varepsilon_0}\right) \quad \ldots\ldots\ldots (3\text{-}6).$$

where C_m is the capacitance of the sensor when the sensor is in contact with the test medium, C_0 is the sensor's capacitance without any test medium, *m* is the relative permittivity of the test medium and *0* is the relative permittivity of air. Thus, sensitivity increases with the increase in the capacitance variation. The sensitivity plot of Fig. 3.2 (b) is directly obtained from equation (3-6), where C_m is calculated from,

$$C_m = \frac{-1}{2*\pi*f*im(z(1,1))} \quad \ldots\ldots\ldots\ldots (3\text{-}7).$$

where, *f* is the operational frequency, i.e. 915 MHz, and *imZ(1, 1)* is the imaginary part of the impedance, that changes with the permittivity of test medium. The sensitivity values obtained using the above equation are $\frac{7.5\ fF}{\%WC}$ and $\frac{4.5\ fF}{\%RH}$ for soil moisture and air relative humidity respectively.

We further extended the sensitivity definition in terms of total change in the phase of the input signal to the total change in the water content or relative humidity. This definition of sensitivity is more specific to our application and provide the actual sensitivity in terms of phase variation. The sensitivity equation is represented by 3-8.

$$S_{\frac{\delta \phi}{\delta WC}} = \left(\frac{\phi_1 - \phi_0}{WC_1 - WC_0}\right) \quad \ldots\ldots\ldots\ldots\ldots (3\text{-}8)$$

where ϕ_1 is the phase value for the highest water content (relative humidity) and ϕ_0 is the phase value for the lowest water content (relative humidity), WC_1 is the highest water content (relative humidity) and WC_0 is the lowest water content (relative humidity).

Based on the above equation the calculated sensitivity values for the water content detection in soil is $\frac{0.27^o}{\%WC}$. As well as the sensitivity in the case of relative humidity detection is $\frac{0.15^o}{\%RH}$. From this equation we can see that the sensitivity of the sensing system can be improved by increasing the overall phase variation of the reflected signal at the input port. Higher phase variation is usually caused by high capacitance variation of the IDC structure.

The resolution of the sensing element for both the soil moisture and air humidity detection can be calculated by using the sensor sensitivity as well as the minimum detectable phase variation, given by 3-9.

$$Resolution = \frac{minimum\ detectable\ phase\ variation}{sensor\ sensitviity} \quad \ldots\ldots\ldots\ldots (3\text{-}9)$$

Based on our measurement setup the minimum detectable phase variation is $\pm 1^o$. Therefore, the proposed sensing element can detect a minimum variation of 7.5% WC and 13.3% RH in the case of water content and relative humidity measurement respectively, based on the calculation below.

$$Res_{(WC)} = \frac{2}{0.27} = 7.5\%\ WC$$

$$Res_{(RH)} = \frac{2}{0.15} = 13.3\%\, RH$$

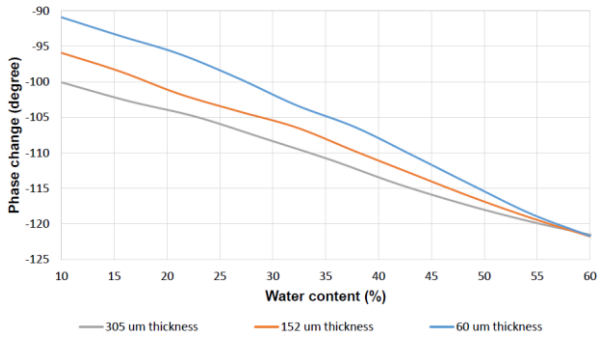

(a)

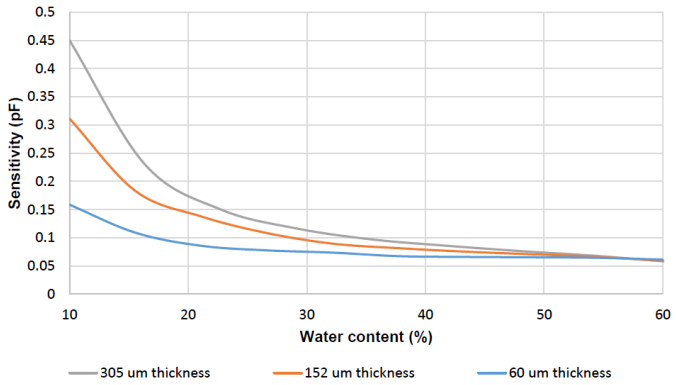

(b)

Figure 3.3. (a) Phase change for different thicknesses of the sensing layer. (b) Sensitivity for three different thickness values of the sensitive layer.

From the above analysis we have seen that the sensitivity can be improved by increasing the overall phase or capacitance variation. The capacitance variation (ΔC) of the IDC is a function of the design dimensions, such as length of the electrode's fingers, width of the finger's gaps between the electrodes and so on. The capacitance

variation can be modified by optimizing these dimensions. This relationship can be represented by the expression 3-10 [81].

$$\Delta C = C \times \left(\frac{\Delta L}{L} + \frac{\Delta W}{W} + \frac{\Delta d}{d}\right) \quad \text{..... (3-10)}$$

Where, C, L, W, and d are the initial values of the capacitance, electrodes length, electrodes width and gap between the electrodes respectively. $\Delta C, \Delta L, \Delta W,$ and Δd are the variations in the capacitance, electrodes length, electrodes width and gap between the electrodes respectively. This expression can be used to obtain multiple values of the capacitance variation and can be utilized to obtain better sensitivity by optimizing the dimensions of the IDC sensing element based on the application requirement. The proposed sensor has been optimized in terms of overall capacitance and phase variation by modifying the structure dimensions using simulations in the electromagnetic cad tools.

3.2. Measurement and Results

3.2.1. Fabrication of IDC Sensor

The structure design and numerical simulations of the IDC sensor were performed using Ansys full-wave FEM simulations. The final design was fabricated using laser LPKF U3 for laser etching and ProtoMat S62 for drilling holes and cutting out the PCB. A 1.52 mm thick Rogers 4003 (double sided 35µm copper) substrate was used for fabrication. Before exposing the substrate to a laser beam for fabrication, the LPKF U3 was first calibrated for the given substrate and copper thickness to avoid

any under or over-etching, that could possibly cause poor fabrication or otherwise damage the substrate. After proper calibration, the IDC structure along with the CPW feed was printed on the top layer and the defected ground on the bottom layer of the PCB. Even though the laser LPKF U3 is capable of drilling holes and cutting the substrate, ProtoMat S62 is selected due to its flexibility and ease of fabrication. The Via holes all over the CPW feed were drilled utilizing a 1mm diameter drilling bit from the ProtoMat toolbox. The Via holes were filled by soldering a wire on both sides of the prototype as shown in Fig. 3.3.

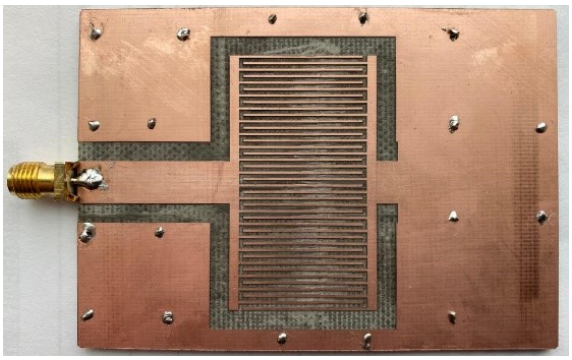

Figure 3.4. Fabricated prototype of the proposed sensor.

3.2.2. Preparation and Deposition of the Sensing Layer

PVA (Polyvinyl alcohol) was used as a sensing layer on top of the interdigital capacitor. The deposition of a sensing layer improves sensitivity to humidity detection because it allows more water particles to accumulate on the surface of the sensing electrodes. The sensing layer was deposited on the sensor using the spray coating technique. The PVA solution was prepared by dissolving powder PVA in deionized water at a ratio of 1:50. The suspension was heated at 150^{o}C and stirred

continuously with a magnetic stirrer for 2 hours until it became completely transparent. After cooling, the solution was sprayed on top of the sensor. Hot air was then used to evaporate the excess water while leaving behind a thin layer of the PVA solution. This process was repeated several times to deposit various sensing layers on the sensor electrodes, each with a particular thickness.

3.3. Results and Discussion

To validate the sensor's performance, the prototype was practically tested for soil moisture content, and air humidity detection. All the measurements were performed using ROHDE & SCHWARZ Vector Network Analyzer (VNA) to estimate the phase and capacitance variation due to the change in the test medium permittivity. Based on the prototype structure, a single port measurement was performed for all three types of experiments.

3.3.1. Soil Moisture Detection

Clay soil with a water content percentage of roughly 20% was used for the laboratory experiments. The initial water percentage in the soil sample was calculated by the ratio of weight of water to the weight of clay soil. These values were calculated by weighting the soil sample before and after drying it in an oven [77]. The sensor phase change and sensitivity were recorded (at 22^{o}C and 44%RH) for a wide range of soil moisture content variations from 20% to 100%. To do so, nine different soil samples were prepared with a moisture content difference of 10% each. These samples were prepared by adding 10% more water each time to the test sample based on the water

content value determined for the initial sample. Primarily the sensor was placed in normal soil (20% moisture) and its response was measured using a vector network analyzer (VNA) at a fixed frequency of 915 MHz as illustrated in the test setup of Fig. 3.4 (a). This process was repeated for every sample by washing and drying the sensor each time after measuring one sample and then placing it in the next sample with higher moisture content. The phase change response with respect to the soil moisture content of Fig. 3.4 (b) shows that there is a linear down shift in the phase change as the soil water content increases. The curve fitting model suggests a linear equation for the measured data with R2 = 0.978. Even though the results are fairly linear, the small non-linearity is due to the fact that the soil samples do not have a homogenous distribution of water content. Also, the gaps between the electrodes of the capacitor are not completely filled with the soil sample, which adds to the uncertainty in the results. However, a sufficient amount of fringing electric fields penetrates the test medium which affects the sensor's capacitance and phase due to the change in water content (permittivity). A comparison between the simulated and measured phase change is shown in Fig. 3.5. The measured phase change is slightly less than the simulations because of the additional parasitic capacitance during experimental measurements that reduces the overall variation in phase. From the experiments, it is clear that the sensor offers good detection sensitivity and linear response to low as well as high water content percentage in soil using the reactive capacitance measurement technique.

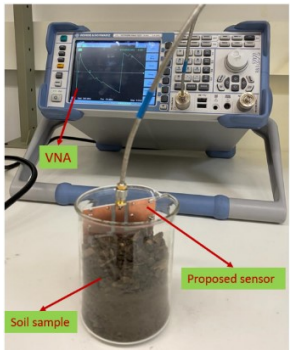

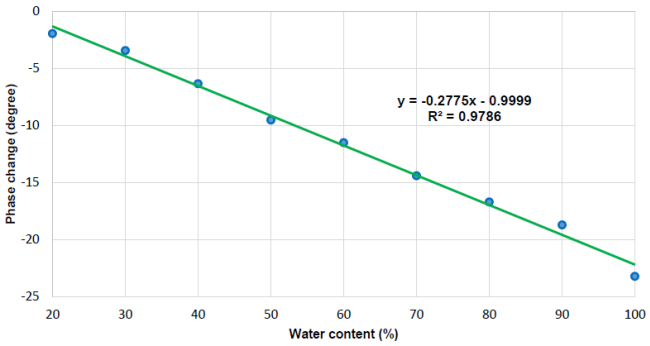

(a) (b)

Figure 3.5. (a) Soil moisture measurement setup. (b) Measured sensor response for soil water content detection.

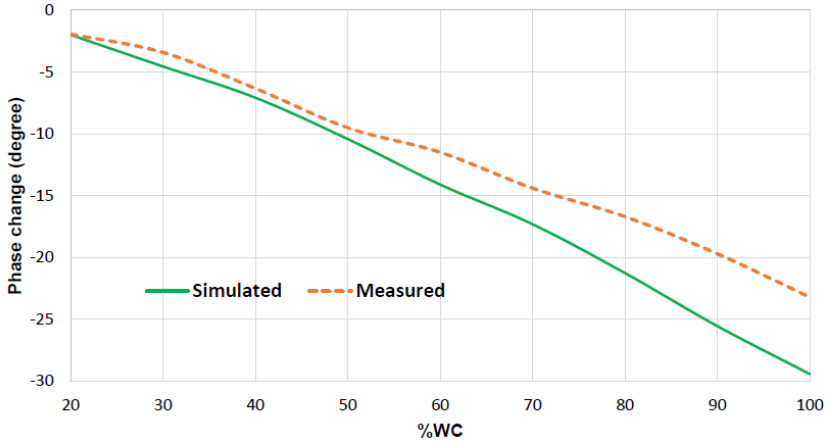

Figure 3.6. Comparison of the simulated and measured phase change response.

3.3.2. Humidity Measurement

The previous measurements were carried out using the proposed sensor without any sensing layer. For humidity detection, the sensor was spray-coated with a PVA layer to increase its sensitivity to air relative humidity (RH). The experimental setup for humidity measurement is shown in Fig. 3.6 (a). In-house humidity chamber was developed for the lab experiments by creating air humidity in the chamber using

Repti-Fogger RF-10 humidifier. The actual humidity was monitored and controlled by a commercially available reference humidity sensor HT-10 from ZOO MED. In order to uniformly distribute the water droplets, a small fan powered by a DC power supply was placed inside the chamber. The variation in phase and capacitance measurements was carried out using a vector network analyzer connected to the single port of the proposed sensor. The sensor performance was recorded at a room temperature (22^{o}C) using a fixed frequency of 915 MHz, for each 10% increase in relative humidity from 30% to 100%. Fig. 3.6 (b) shows a comparison of the phase change with respect to humidity for a sensor with five different sensing layer thickness. It is evident from the measured results that, with the increase in sensing layer thicknesses, the overall sensitivity increases, although, the response rate of the sensor decreases. Additionally, unlike the soil moisture and liquid level detection, the curve fitting to the measured data for humidity with a sensing layer thickness of 110 μm is not linear but a polynomial fit with R2 = 0.990. The reason for this is the smaller capacitance and phase change at lower humidity level (below 65%) due to the less dependence of humidity and slower response time. Another reason for non-linearity at a low RH level is the limitations of the experimental setup, which cannot hold a constant humidity level for a long time such that the sensing layer adsorbs enough water molecules. The water molecule either escapes the chamber or settles down on the surface. This measurement error can be reduced by using a commercially available humidity chamber and sensor with a thin sensing layer and fast response time. Similar non-linear behavior at the low humidity level has been reported in the literature for IDC sensors. In [78] the impedance response of an IDC based humidity

sensor is analyzed for different types of sensing materials. The impedance response is only linear for higher humidity levels, but non-linear for the different percentages of lower relative humidity depending on the types of sensing material used. Therefore, the article proposes a linear combination of sensors using an array signal processing technique to get a linear response over the full sensing range. Another thin-film miniature IDC sensor is reported for humidity sensing with a linear capacitive response only in the range of 50-80% [79]. The sensor response is non-linear for RH values below 50% and above 80%. Our proposed sensor has a linear capacitance and phase change between 65-100% RH as illustrated in Fig. 3.7 (a). Measured results have also been validated by comparing with the simulation results as shown in figure 3.7 (b). Both the results are in good agreement, except some small discrepancies at the mid-range humidity level, although the overall phase change is similar in both cases.

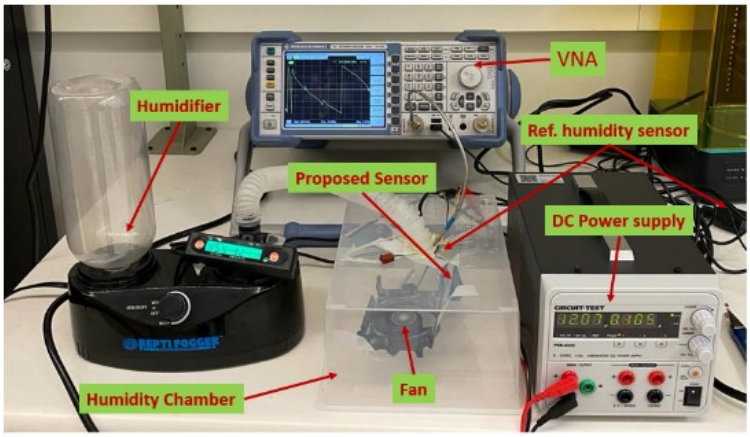

(a)

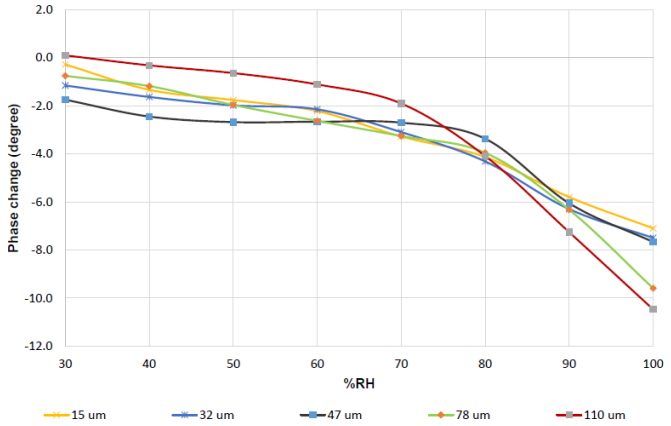

(b)

Figure 3.7. (a) Experimental setup for humidity measurement. (b) Phase change with respect to relative humidity for various sensing layer thickness.

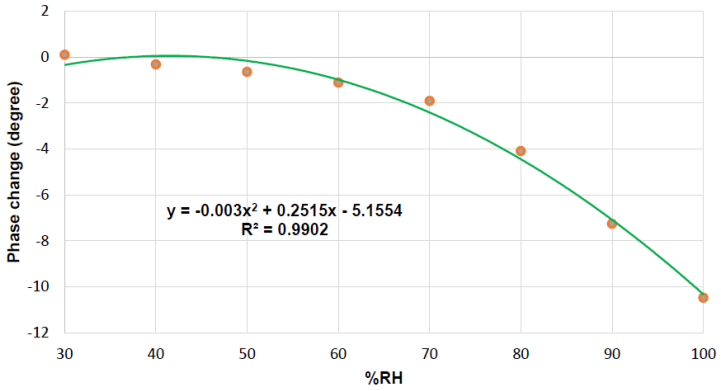

(a)

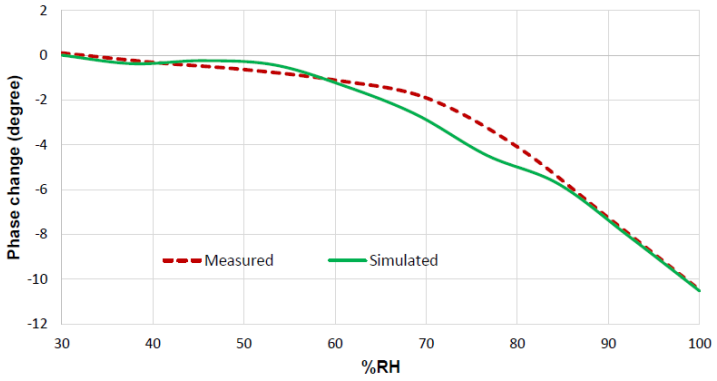

(b)

Figure 3.8. (a) Polynomial curve fit for measured data using 110 µm thick sensing layer. (b) Comparison of simulated and measured phase change with respect to relative humidity.

An overview of the proposed sensor in comparison with other sensors described in the literature can be found in Table 3.1. The major differences are related to the type of sensing material used, the sensing range, the parameters to be measured, and the shape of the response curve. The proposed sensor can measure three different parameters with linear responses for measuring moisture and liquid level and almost linear responses for measuring humidity for a wide range of measurements. Furthermore, this sensor has an excellent reliability and can be used in zero-power battery-less RFID sensing architectures.

Table 3.1. Comparison of the proposed sensor with other similar sensors.

Refs.	Sensor type	Sensing Material	Fabrication method	Sensing parameters	Sensing range (%)	Curve shape
[21]	Interdigitated electrode	MoSe2:PVOH	Screen printing & spin coating	Humidity	0-100	Linear
[82]	Interdigitated electrodes	GaN powder	Spin coating	Humidity	11-95	Non-linear
[10]	Microstrip resonance ring	-	-	Moisture	0-20	Almost linear
[83]	Diode formation	ZnO/Porous GaN	Chemical etching & spray coating	Humidity	12-96	Non-linear
[84]	Resistive sheet formation	β-Ga2O3 nanowires	MOCVD	Humidity	35-95	Linear
[14]	Interdigitated electrodes	-	-	Moisture	0-40	Non-linear
This work	Interdigitated electrodes	Polyamide (PVA)	Spray coating	Moisture/Humidity/Level	20-100 (Soil moisture) 30-100 (Humidity) 0-5mm (Level)	Linear (Moisture) Almost linear (Humidity) Almost linear (Level)

3.4. Summary

This chapter presents the design of a novel interdigitated capacitive sensing element based on grounded coplanar waveguide feed with a capability to be integrated with a passive wireless RFID sensing architecture. The sensing principle is based on the phase change of the RF input signal as a function of the test medium permittivity due to the variation in reactive capacitance of the sensing element. The proposed capacitive IDC element is practically tested for soil moisture, and air humidity in a laboratory environment. All the experiments were performed at room temperature of

22^{o}C. Results show that the sensor without any sensing layers exhibit low sensitivity to relative humidity. In order to increase sensitivity, the polyamide spray coating is used. A humidity chamber within the laboratory was used to expose the sensor to variations in air RH from 30 to 100%. The linear phase variation response is observed in the RH levels ranging from 65 to 100%.

Chapter 4 Wireless capacitive liquid level detection sensor based on zero-power RFID sensing architecture

Detection of liquid level is a key sensing technique driving several technological industries, however, as discussed in chapter 2, most of the sensors designed for this application suffers from limitations such as power inefficiency, low reliability, complexity and in some cases, they lack the capability of wireless transmission, which limited their use for several applications.

This chapter is focused on the design of a new type of wireless liquid level detection sensor as shown in Fig. 4.1. The working principle of the sensor is based on a variation in fringe capacitance that changes the reactive phase of the backscattered signal, due to changes in the liquid level; which is detected by the RFID reader. A high phase transition is caused by the resonance frequency shift at 927 MHz; due to changes in the reactive capacitance of the sensing element. Reactive phase change measurement is simple, inexpensive, and offers some additional advantages such as short response time, stability, and low power consumption that could solve most of the limitations of the currently available level sensors. The proposed liquid level detection system increases the reliability of the current sensors by integrating a highly linear capacitive element with a passive sensing node to reduce periodic maintenance, cost, design complexity and to increase sensitivity and measurement linearity.

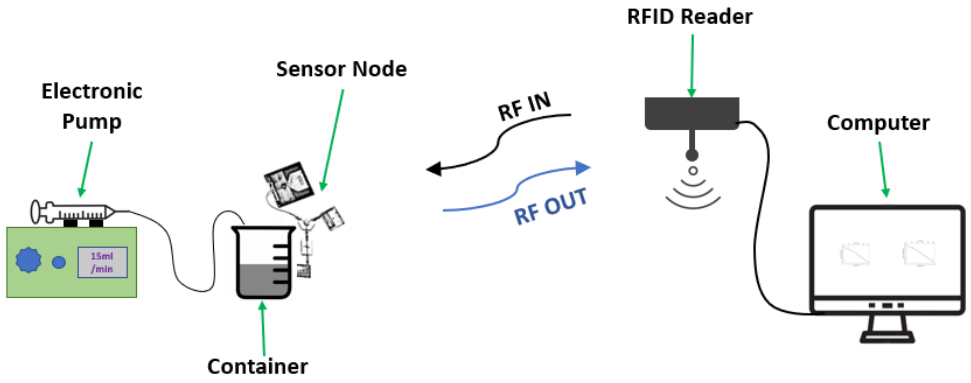

Figure 4.1. Demonstration of the proposed wireless liquid level measurement system.

4.1. Theory

4.1.1. Sensor Architecture

The proposed sensing method integrates a capacitive sensing element with a passive three-port UHF RFID architecture to develop a wireless liquid level detection system. The three-port architecture is previously developed and is tested for other sensing applications [43][85]. The sensing system comprises of a circulator, a filter, a UHF RFID chip and antenna as shown in Fig. 4.2. Due to the non-reciprocal nature of the circulator, the signal received from the reader by the antenna is sent to the RFID chip for excitation. Upon energizing, the chip reflects a backscattered signal which is then diverted to the reactive sensing element through a bandpass filter. The sensing element adds a phase delay to the signal in the passband (927 MHz) based on the information from the liquid level height, which is received by the reader. The phase of the reflected frequencies in the filter stopband is used as a reference to calculate the phase difference caused by the change in the liquid level. These backscattered signals when received by the reader are used to generate an IQ signals with the help

of a built-in noncoherent IQ demodulator. By programing the reader, the phase delay caused by the sensing element due to the variation in the liquid level can be determined by subtracting the phase delay of the pass-band frequencies from the reference phase of the reflected signals. The reference phase is helpful to remove any phase ambiguity due to the distance of the wireless node from the RFID reader as well as the phase delay added by various components in the architecture. The reference phase in the filter stop-band also reduces the measurement uncertainties caused due to the reflections from obstacles and simplify the measurement method by eliminating the need for distance specific calibration.

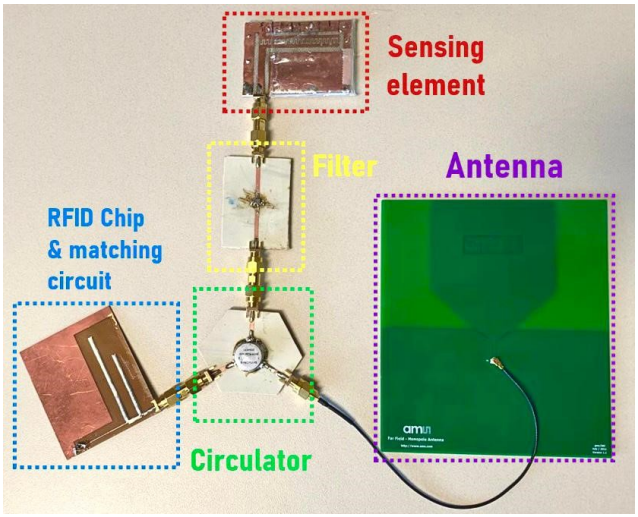

Figure 4.2. Three port RFID sensing node.

4.1.2. Sensing Element Design and Specifications

A detailed design and analysis of the interdigitated electrode sensing element is presented in chapter 3. In this chapter, the IDC structure is further modified and its performance is studied for remote liquid level detection by integrating with a passive

RFID architecture. In addition to other sensing applications, IDC capacitors have been used for liquid level detection [86-88]. The corresponding change in the capacitance of these structures can be used to determine the changes in the material under observation, as represented by the expression 3-1 in chapter 3. The capacitance variation, however, needs to be converted to a measurable parameter such as current, voltage etc. using an additional signal processing circuit that requires an extra amount of power to operate. Thus, an internal power source is needed to drive these circuits that increases the cost and complexity of the sensor nodes. Since, RFID based sensing can utilize phase variation as a sensing parameter without the use of any additional circuitry, therefore, our focus is to optimize phase variation caused due to the corresponding changes in the capacitance of the interdigitated electrode structure. Usually there is a high phase transition associated with the resonance frequency shift. The designed sensing element is optimized to have a resonance at 927 MHz frequency, the magnitude of which changes due to the variation in the liquid level. We exploit the high phase transition caused by the variation in the magnitude of the sensing element's resonance as a sensing parameter to detect changes in the liquid level by integrating the IDC structure with an RFID based sensing architecture.

The sensing element is designed using grounded coplanar waveguide (GCPW) feeding as shown in Fig. 4.3. The structure is designed and optimized using Ansys full-wave FEM software on a Rogers RO4003 substrate (ε_r=3.55) with an overall dimension of 57 mm x 40 mm x 1.6 mm. Electrode fingers with positive potential are fed by the feedline while the negative electrodes terminal is directly shorted to the ground. The active part of the sensor is coated with approximately 600 µm thick

polyethylene layer to make it suitable for use in both conductive and non-conductive type liquids as well as to use it as a contact or a non-contact sensor. The optimized design is fabricated using an LPKF U3 laser-based and mechanical-milling based ProtoMat S62. Fig. 4.4. shows a simplified schematic of the proposed sensing element with the representation of the fringing fields passing through the test medium.

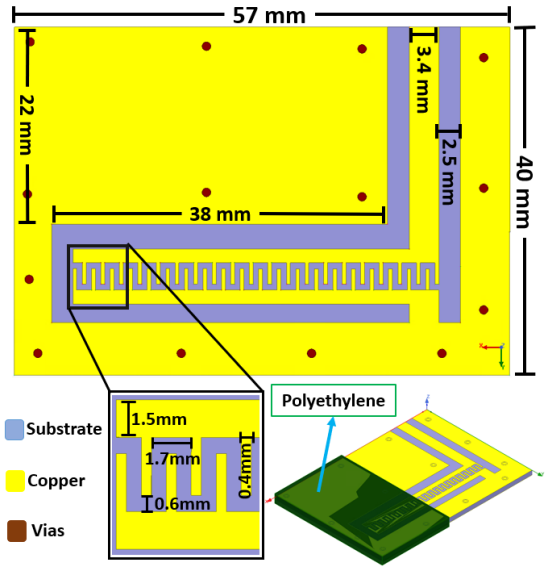

Figure 4.3. Diagram of the proposed sensing element.

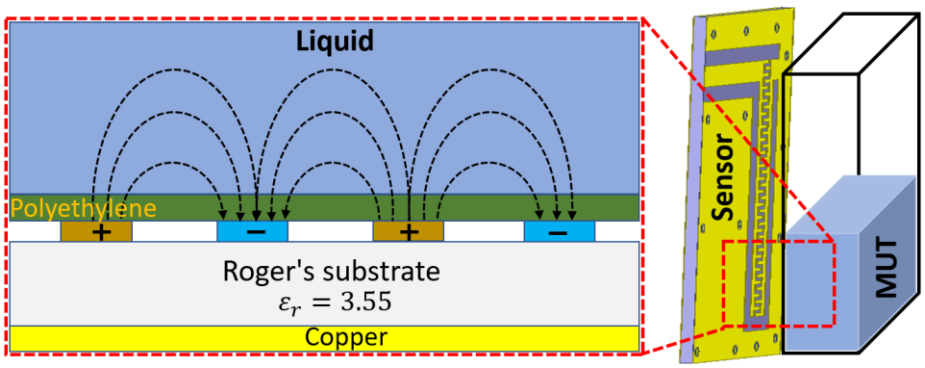

Figure 4.4. Schematic representation of the sensing element.

4.2. Results and Discussion

The feasibility of the proposed system was tested by implementing the model in Keysight's advanced design system (ADS). The sensing element was designed, simulated and optimized using Ansys full-wave FEM simulations to have high linearity, maximum sensitivity and fast response to change in the liquid level. In the simulation model, phase variation with respect to liquid level was plotted at a fixed UHF frequency of 927 MHz.

The sensing element was then integrated into the wireless sensing architecture described in Sec. 4.1.1 for real-time measurements of liquid level in a real-life scenario. The experimental setup in Fig. 4.5. shows a sensor node placed at a distance of about 2 m (measurements up to approximately 7m is possible) from the RFID reader. The sensing element was fixed inside a transparent liquid container and marked with a millimetre scale to detect the liquid level height. Liquid level inside the container was varied in a controlled environment using an electronic syringe pump (IPS-14RS) and pipes to add/remove liquid to/from the container. Tape water was used for all the experiments at a room temperature of 22 ^{o}C. Change in the phase value observed by the sensor is sent wirelessly to the RFID reader through an antenna connected to the port 1 of the circulator. AS3993 Fermi RFID reader used for this experiment, generates IQ signals from the received backscattered signal utilizing a mixer, that is used for determining the phase variation due to changes in liquid level. The reader is programmed in a way to plot the phase variation due to changes in the liquid level by subtracting the phase delay caused by the sensing element from the reference phase.

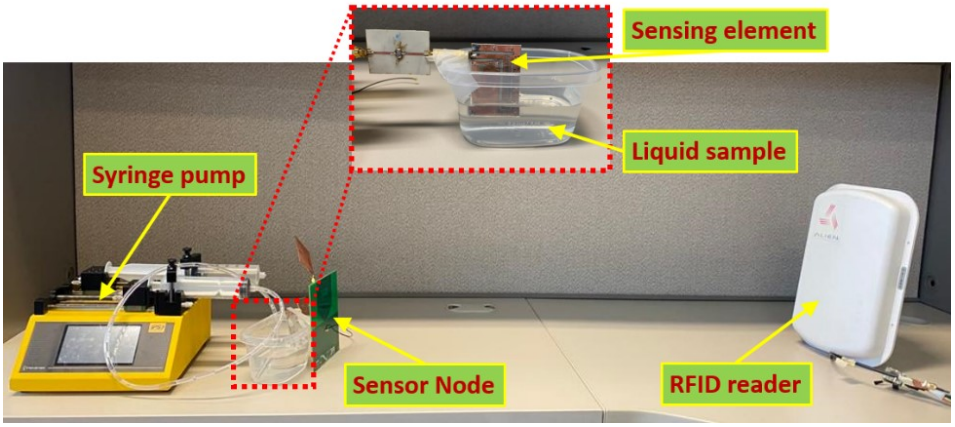

Figure 4.5. Experimental setup for wireless liquid level measurement.

Fig. 4.6. shows the phase variation of the recorded backscattered signal at the reader as the liquid level changes. The initial sensor phase value was 20 ^{o}C at 0 mm liquid level which is linearly downshifted to -23^{o} for a liquid height of 20 mm. Sensitivity of the sensor was found to be 2.15^{o}/mm, which makes the sensor highly efficient for a wide range of applications. The sensor's sensitivity to liquid variation depends on the polyethylene coating thickness over the sensitive part. Sensitivity increases with decrease in thickness of the polyethylene layer due to the increased number of fringing electric fields passing through the test medium. A comparison between the simulated and measured phase variation with respect to liquid level demonstrates a good agreement between both the results. The phase change in the simulations, however, is slightly higher than the measured results because of the additional parasitic capacitance during experimental measurements that reduces the overall phase variation of the sensor.

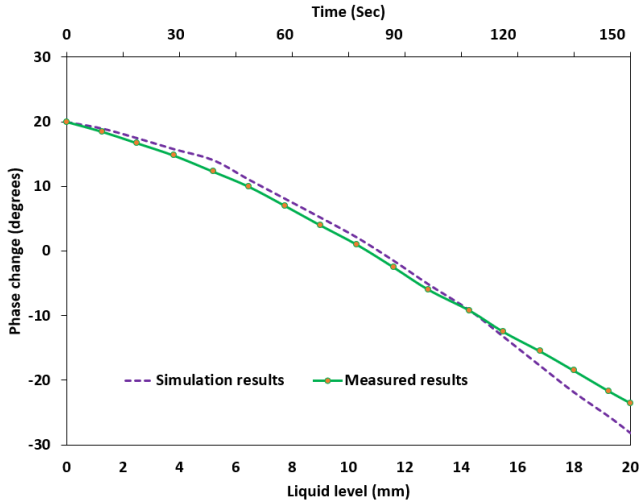

Figure 4.6. Sensor phase variation of the backscattered signal (measured) with respect to liquid level and Comparison of the simulated and measured phase variation.

A repeatability measurement of liquid level sensor is important to ensure proper operation over an extended period of time. A repeatability test was performed by increasing/decreasing the liquid level multiple time and plotting the phase variation with respect to time as well as liquid height, as shown in Fig. 4.7. The sensor phase change due to liquid level was recorded at a fixed passband frequency of 927 MHz (pink). Phase value at two stopband frequencies of 902 MHz (green) and 905 MHz (blue) are also included, indicating a constant phase value according to the architecture design principle. The sharp edges of the triangular style graph at the maximum and minimum level indicate that the direction of phase changes abruptly when the liquid direction is reversed. Thus, the sensor offers good repeatability as well as fast response to change in the liquid level.

Furthermore, some additional tests were performed to ensure that the sensor can hold a constant phase value for different liquid heights. Fig. 4.8. shows the phase variation of a backscattered signal by increasing and holding the liquid level at different heights. During each hold the liquid level was kept constant for roughly 60 sec and then increased in steps with a step size of 5 mm. From the figure it can be seen that the sensor phase is constant when there is no change in the liquid level and decreases linearly with an increase in the liquid height. These experiments confirm that the proposed sensor can detect any height within the measurement range. Therefore, it can be used as a point level detector as well as a continuous level measurement wireless sensor.

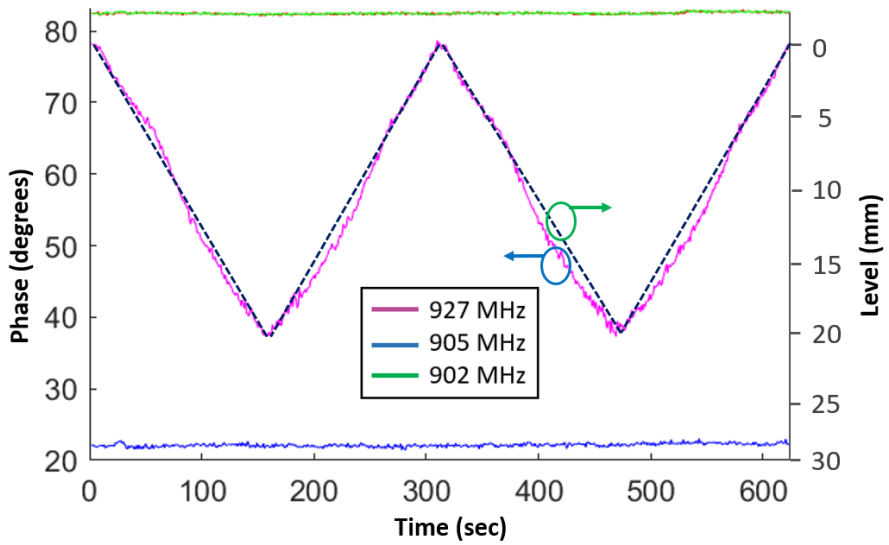

Figure 4.7. Repeatability test results of the proposed sensor.

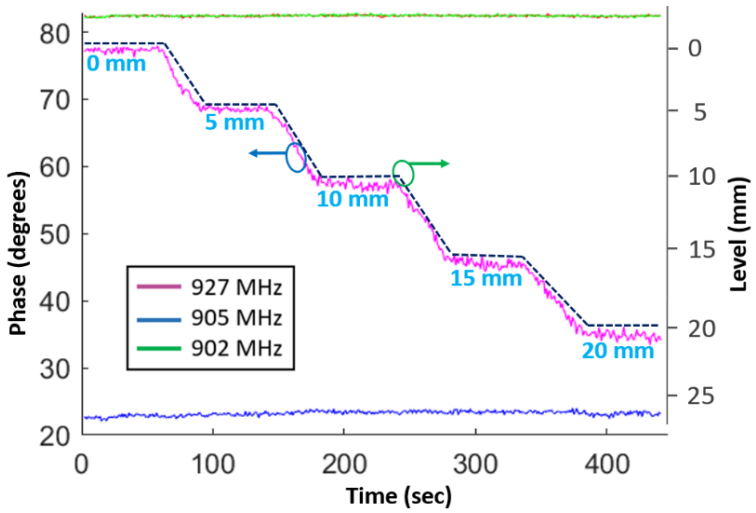

Figure 4.8. Sensor phase variation w.r.t change in the liquid level in steps.

A comparison of the proposed wireless sensing method with other liquid level detection sensors is given in Table 4.1. The sensor can detect liquid level wirelessly from a remote location with high linearity. By using the phase of the RFID signal as a sensing parameter, the complex signal conversion circuits at the sensor node are avoided to reduce the cost and complexity of the proposed level sensor. The sensitive part of the sensor is coated with a polyethylene layer, making it capable to be used as a contact or a non-contact sensor in conductive or non-conductive type liquid. During contact sensing, the liquid is in contact with the polyethylene coating only, with no direct contact with the electrodes of the IDC structure, that reduces the dependence of the sensor performance on the liquid properties. The sensor has also the capability to be used as a non-contact sensor (if needed) placed outside of the liquid container using the effect on the fringing electric fields due to change in the liquid level as a sensing parameter. Additionally, the polyethylene coating removes the hysteresis

effect due to its smooth surface that does not allow any liquid to accumulate on the surface of the sensing element, especially, when the liquid level is dropped, thus providing excellent repeatability. Although the sensor is designed to detect changes in the liquid level for up to 20 mm, it can fulfil the requirements of the current and future this class of sensing applications in a densely populated wireless environment. The detection range can be easily extended from 20 mm to several centimeters by cascading the proposed sensing element design.

The sensitivity of the proposed sensor can be represented as the ratio between the overall phase variation and the total change in the liquid level.

$$S_{\frac{\delta\phi}{\delta h}} = \left(\frac{\phi_1 - \phi_0}{h_1 - h_0}\right) \quad \text{..... (4-1)}$$

Where, ϕ_0 is the initial phase value at liquid height h_0 and ϕ_1 is the final phase value at a liquid height h_1.

Based on the above equation, the proposed wireless liquid level detection sensor offers a sensitivity of $2.15^{\text{o}}/\text{mm}$. The sensor resolution can also be calculated using the sensitivity information and the expression introduced in chapter 3 as follows.

$$Resolution = \frac{minimum\ detectable\ phase\ variation}{sensor\ sensitviity} \quad \text{..... (4-2)}$$

The RFID reader used for these experiments has a phase detection accuracy of about $\pm 1^{o}$, therefore, the resolution of the proposed sensor is calculated to be 0.9 mm. Which shows that the sensor can accurately detect a liquid variation of as small as 1 mm.

Table 4.1. Comparison of the proposed wireless sensor with other liquid level detection sensors.

Refs.	Sensing element	Complexity	Self-powered	Wireless	Measurement type	Sensitivity (/mm)
[89]	Impedance phase	Moderate	No	No	Contact	0.21°
[30]	Resonance	Low	No	No	Non-contact	-
[90]	Capacitive	Moderate	No	No	Contact	40.26 fF
[91]	Magnetic coupling	Moderate	Yes	Yes	Contact	-
[92]	Resistive	Moderate	No	Yes	Non-contact	8.75 Ω
[93]	Capacitive	Low	Yes	Yes	Contact/Non-contact	-
[94]	Coaxial cylindrical	Low	No	No	Contact	1.05 pF
This work	Reactive phase	Low	Yes	Yes	Contact/Non-contact	2.15°

4.3. Summary

This chapter proposes a new method for wireless liquid level measurement using a three-port UHF RFID sensing architecture and a capacitive sensing element. The reactive capacitance of the sensing part changes with the liquid level variation. A high phase transition associated with the change in the reactance, is used as a detection parameter by the RFID sensor for liquid level measurement. The active part of the sensor is coated with approximately 600 µm thick polyethylene layer, making it suitable for use in both conductive and non-conductive type liquids as well as the sensing element of the sensor can be placed within or outside the container. Experimental results demonstrate a linear phase change response with a high sensitivity of $2.15^0/\text{mm}$. All the experiments were performed at a room temperature. The proposed sensor offers reliability, real-time response, linearity, high sensitivity and excellent repeatability, making it capable of use in a wide range of applications especially IOT based sensing environment.

Chapter 5 Volumetric characterization of multivariable mixtures using RFID based passive wireless capacitive sensor

In chapter 4, a remote liquid level detection system using a three-port UHF RFID architecture has been introduced. The sensing system is further modified by designing and integrating a new sensing element with the RFID architecture to devise a new sensing technique for the volume fraction analysis of a binary and multivariable liquid mixture samples remotely in real-time.

Based on our proposed method, Multiple sensing information can be obtained in real-time by analyzing phase of the backscattered signal for various samples at only one frequency and multi-temperatures when the frequency band is limited to solve the multivariable equations. The concept is validated by testing the sensor with sample mixtures having different mixing ratios of three materials (isopropyl alcohol, water and Oil) at a fixed RFID frequency of 927 MHz and two temperatures of 22 ^{o}C and 40 ^{o}C. The volume fractions were numerically investigated by solving the linear system of equations realized using the obtained sensing parameters. A promising accuracy with a mean absolute error of less than 4.6% can be achieved for the volume fraction measurement of the test samples. The proposed sensor will facilitate improvement in the volume fraction analysis of multivariable mixtures by eliminating the internal power source and complex signal processing circuits from the wireless sensing node to provide power efficiency, reliability and reduced maintenance for widespread real-time sensing.

5.1. Sensor Design and Working Principle

5.1.1. Sensor Node Design

The three-port UHF RFID sensing architecture discussed in chapter 4 is used for the proposed sensing method. A new sensing element is designed on a Rogers RO4003 substrate (ϵ_r= 3.55, h = 1.52 mm, tanδ = 0.0027) with an overall dimension of 57 mm x 40 mm x 1.6 mm and optimized using Ansys full-wave FEM software as shown in Fig. 5.1. Capacitance based sensing element is selected due to their minimal resistive part that increases energy efficiency and are considered a good option for passive wireless sensor platform. The corresponding change in the capacitance of these structures is used to determine changes in the property of a material under observation, e.g. permittivity variation (ϵ). Conventionally, an additional signal processing circuit is used to convert the capacitance variation to a measurable quantity such as current, voltage etc. which increases the system cost and complexity. Since, in our case, the capacitance variation also alters phase of the input signal, we use phase variation as a sensing parameter by utilizing RFID architecture without the use of any additional signal processing circuitry to reduce design complexity, cost, and to improve power efficiency. The proposed sensing system for volume fraction measurement utilizing a three-port RFID architecture and a capacitive sensing element is shown in Fig. 5.2.

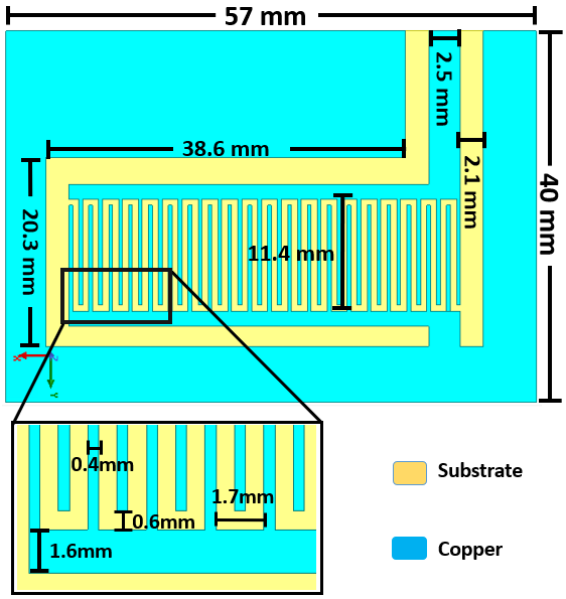

Figure 5.1. Diagram of the proposed sensing element.

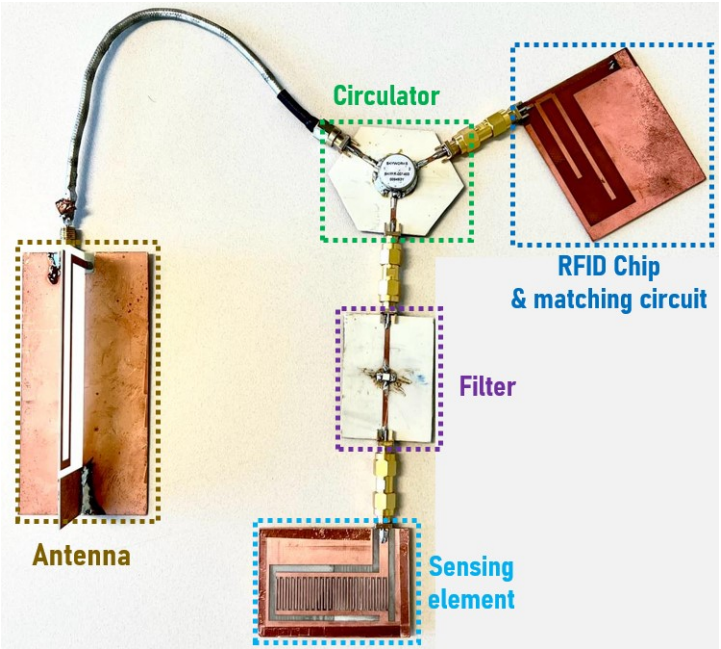

Figure 5.2. Three port RFID sensing node design.

5.1.2. Principles and Operations

The interdigitated electrode capacitive sensing element transduces changes in the properties of the material under test (MUT) into a corresponding change in the capacitance. The materials of interest used for the preparation of the test samples are isopropyl alcohol, water and vegetable Oil, that are chosen based on the sensor application. Vegetable oil is selected for simplicity due to the fact that its permittivity is closer to the permittivity of crude oil. Since the permittivity profile of each component is different, a unique set of real effective permittivity for various sample mixtures can be obtained based on the materials mixing ratio. Upon exposing the sensor to the liquid samples, different capacitance values can be obtained according to the well-known IDC capacitance equation introduced in chapter 3 [73].

The expression shows a direct relationship of the material permittivity and the IDC sensor capacitance, thus, providing high sensitivity. The sensitivity is defined as the shift in the input signal phase due to the difference in the real permittivity of the MUTs. Based on our proposed method, the variation in capacitance introduces an additional phase delay to the input backscattered signal at a fixed frequency of 927 MHz, which is received back by the RFID reader for extracting the sensing information. The sensing principle is based on the variations in the real permittivity only (using non-contact measurements at a fixed frequency), therefore, the analysis of the liquid samples with the tedious, complex permittivity models such as Cole-Cole model [95] and Debye relaxation model [96] are avoided. Since the sensing parameters obtained using a single frequency measurement is not sufficient for calculating the volume fractions of the three unknown materials in a mixture,

therefore, additional sensing information is required. Although, due to the limited RFID frequency bandwidth, multi-frequency measurements are not possible therefore, phase measurement at a single frequency and two different temperatures were carried out due to the fact that the permittivity profile of some components in a mixture is affected by temperature variation that changes the overall effective permittivity of the sample solution. The phase response of the sensor is recorded by introducing the known pure materials, in order to obtain the calibration data to complete the measurement equations for volume fraction calculation. The phase response of the sensor node for each of the pure materials (Oil, Alcohol, and Water) at room temperature is shown in Fig. 5.3. Two independent equations can be obtained by using the measured phase information for each sample solution at two temperatures such as 22 ^{o}C and 40 ^{o}C. Additionally, a 3rd equation can be achieved by considering the sum of the liquid mixture volume equal to unity. Thus, a system of three linear independent equations can be realized for solving the problem with 3 unknowns as given in (5-1),

$$\begin{cases} V_{Oil} + V_{Alcohol} + V_{Water} = 1 \\ \Delta\Phi_{O,T_1} \times V_O + \Delta\Phi_{A,T_1} \times V_A + \Delta\Phi_{W,T_1} \times V_W = \Delta\Phi_{T_1} \\ \Delta\Phi_{O,T_2} \times V_O + \Delta\Phi_{A,T_2} \times V_A + \Delta\Phi_{W,T_2} \times V_W = \Delta\Phi_{T_2} \end{cases} \quad \ldots\ldots (5\text{-}1)$$

Where, subscripts, O, A, and W representing Oil, Isopropyl Alcohol, and Water respectively. T_1 and T_2 represents 22 ^{o}C and 40 ^{o}C temperatures, respectively. $\Delta\Phi_x$ represents the phase shift related to pure material x at the given temperature and V_x is the volume fraction of the material x in the mixture to be determined.

It is also important to notice that results from the experiments can be directly inserted into the above equations. The only unknown variable here is the volume concentration of the mixture components. The phase response of a bare sensor is used as a reference value that helps in calculating the phase difference ($\Delta\Phi_x$) for each sample from a fixed value, making the measurements irrespective of the phase value itself, which reduces measurement uncertainties.

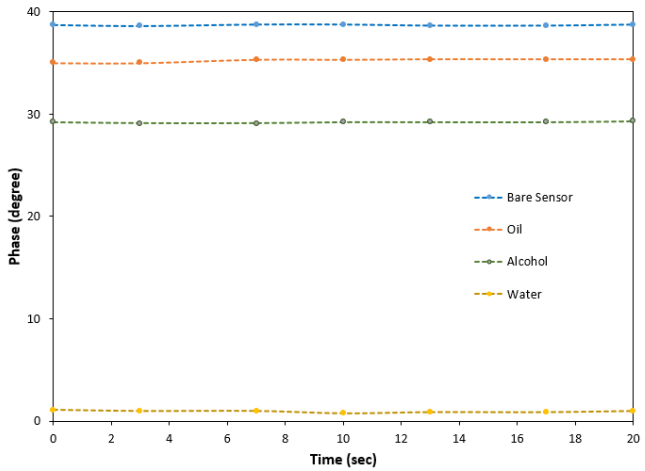

Figure 5.3: Phase versus time curves for the three pure materials at 22 ^{o}C.

5.2. Results and Discussion

The experimental setup for wireless measurement of the volumetric concentration of the unknown samples is shown in Fig. 5.4. The sensing element is attached to the side of a plastic container with a wall thickness of about 0.2 mm. Sensor node is placed at about 2 meters distance from the RFID reader, with a maximum range capability of approximately 7.5 meters according to the proposed sensing architecture. A 130 ml volume of each sample (pure materials and mixtures) was selected in a way that the sample covers most of the area of the sensitive part of the sensor. Since the

components of the mixture does not completely mix with each other (especially water and Oil) during normal condition, an electromechanical mixer is used to prevent materials from separation. Thus, due to the constant functioning of the mixer, the sample mixtures are considered to be almost homogenous. The sensor was introduced to various samples and the phase variation of the backscattered signal was recorded at the RFID reader which is then displayed on the computer screen. The reader used for these experiments is AS3993 Fermi, that generates IQ signals from the received backscattered signal by utilizing a mixer, that determine the phase variation due to the variation in the permittivity of the MUT. As discussed in Sec. 5.1, the phase analysis of each sample was performed at two temperatures (22 ºC and 40 ºC). In order, to heat-up the samples, a 4-ohm ceramic resistor (UB5C-4RF), powered by a DC power supply is used as a small heater placed close to the sensing element. It is sufficient to heat the liquid sample around the vicinity of the sensing element only for power efficiency. A reference temperature sensor is used to control the heating and take the measurements once the temperature reaches 40 ºC. Thus, two phase measurements are realized at a low and high temperature, respectively, without changing the sample inside the container.

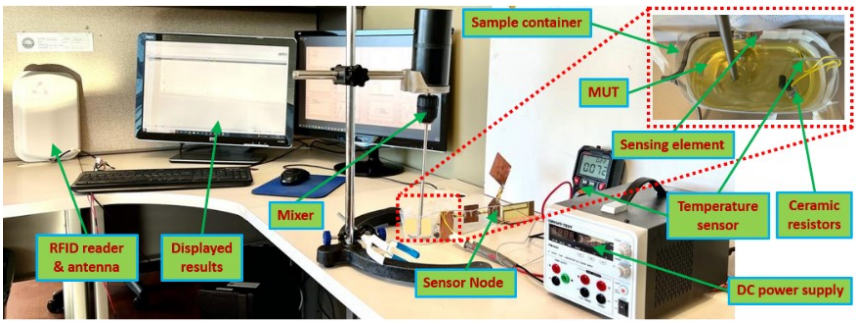

Figure 5.4: Experimental setup for wireless volume fraction analysis.

The feasibility of the proposed sensor was first evaluated with a binary sample by mixing different ratios of water and Oil at room temperature as plotted in Fig. 5.5. Six different samples were prepared with the increase of 20% water concentration from sample 1 to sample 6. A linear downshift in the phase values versus permittivity can be observed at the RFID reader as the water concentration increases from 0% (pure Oil, ϵ_r = 3.1) to 100% (pure water, ϵ_r= 79) at 927 MHz. These results demonstrate that the sensor works very well for calculating the water concentration in Oil, for both low and high water volume fractions in real-time.

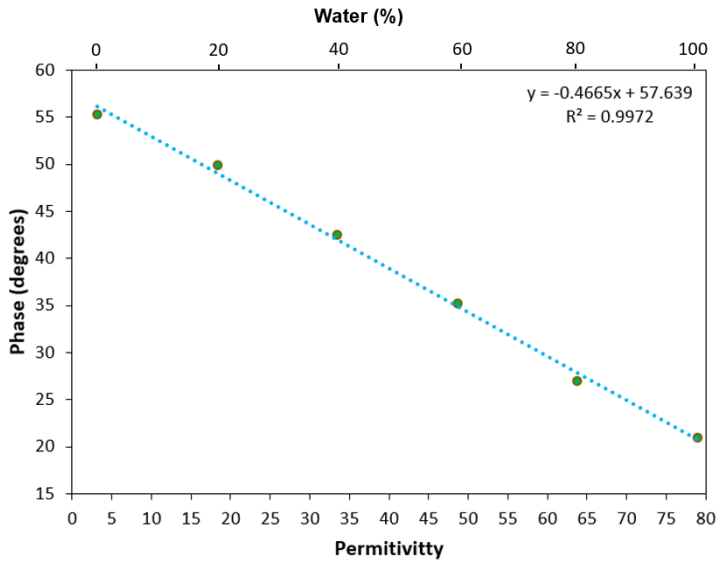

Figure 5.5: Phase with respect to permittivity for various concentrations of water in Oil.

The volume fraction calculation in a multivariable mixture, however, is not very straight forward and require further analysis of the sensing parameters obtained from the multi-temperature measurement of the sensor. Based on our experiments, each sample contains three components with unknown concentrations, therefore, three

independent equations are required to calculate their volume fractions. Due to the unique permittivity profile of every component the resultant effective relative permittivity of the sample mixture is unique for different mixing ratios as represented by (5-2). Thus, by calculating the phase values for every sample at 22 ^{o}C and 40 ^{o}C, two independent equations can be obtained as given by (5-1). According to the literature [97], water has the maximum change in the real permittivity profile with variation in temperature from 22 ^{o}C (ϵ_r= 79) to 40 ^{o}C (ϵ_r= 73), that causes a significant change in the overall effective permittivity's of the samples. The permittivity value of Oil, on the other hand, is almost constant with the increase in the temperature. For isopropyl alcohol the small change in the real permittivity causes a negligible phase variation by increasing the sample temperature from 22 ^{o}C and 40 ^{o}C. This analysis further simplifies the problem by considering the phase difference between the lower and higher temperature for a specific sample is caused by the variation in the permittivity of water alone. Therefore, the volume fraction of water can be calculated first, followed by Oil and Alcohol by solving the linear system of equations.

$$\epsilon_{reff} = V_O \times \epsilon_{r,O} + V_A \times \epsilon_{r,A} + V_W \times \epsilon_{r,W} \qquad \text{..... 5-2}$$

Where, V_O, V_A, and V_W represent the volume fractions of Oil, Alcohol and Water, respectively and $\epsilon_{r,O}$, $\epsilon_{r,A}$, and $\epsilon_{r,W}$ are the individual real permittivity's of Oil, Alcohol and Water, respectively.

The equation system given in (5.1), contains three types of data; the unknown volume fractions of each subcomponent in a sample, the calibration data that can be obtained

by loading the sensor with pure materials, and the phase variation information for each mixture MUT that can be achieved by taking the phase measurements at two temperatures by loading the sensor with the samples. Fig. 5.6 and 5.7 show the sensor phase values recorded at the RFID reader for the four unknown samples at 22 ^{o}C and 40 ^{o}C, respectively. For each sample phase of the input signal is plotted versus time for 20 seconds. Since the RFID reader displays phase versus time measurements with some variations in the phase values, therefore, seven data points are considered within the 20 sec time frames to calculate the mean phase values for each test sample. The deviation from the mean values are used to calculate the variance in the measurements for every sample as represented in Table 5.1.

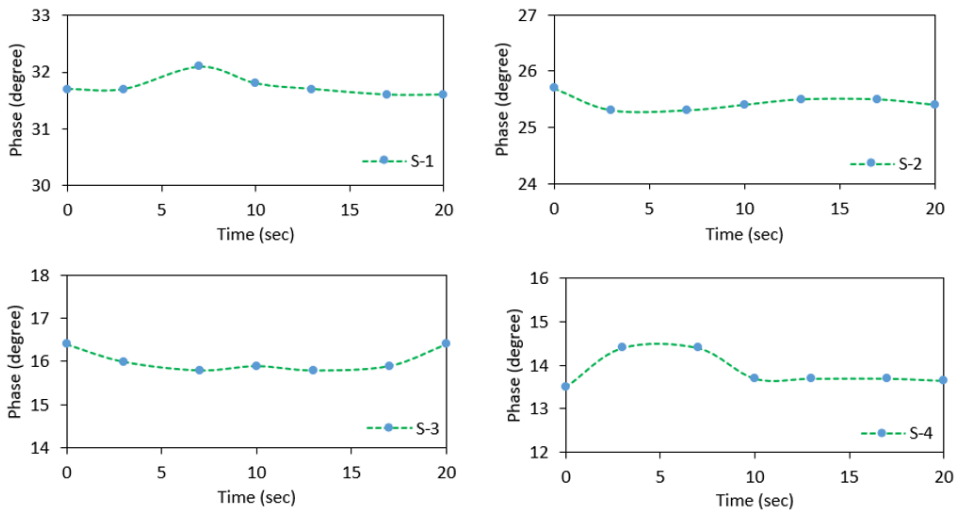

Figure 5.6: RFID phase versus time plots for various samples at 22 ^{o}C.

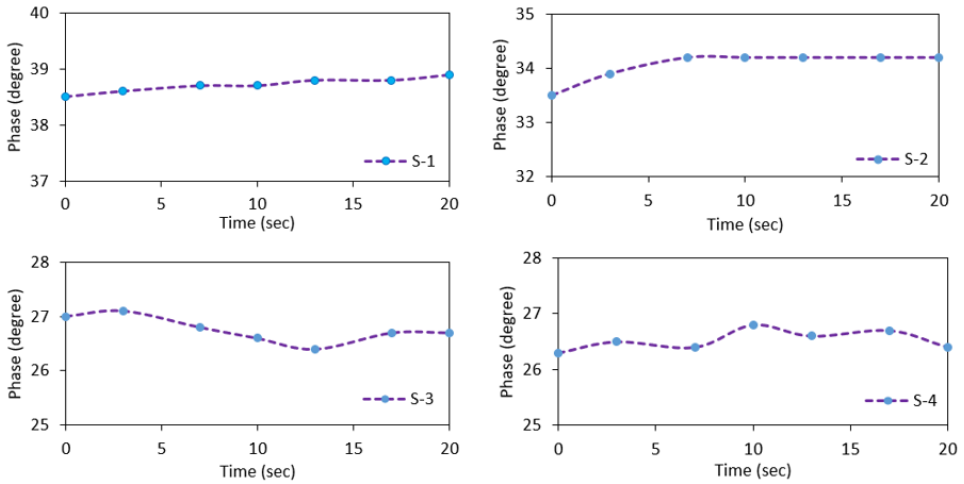

Figure 5.7: RFID phase versus time plots for various samples at 40 ºC.

TABLE 5.1: Sensor phase and variance values for each sample.

Sample	Phase value (22 °C) (degree)	Variance (22 °C) (σ^2)	Phase value (40 °C) (degree)	Variance (40 °C) (σ^2)
Air	38.7	0.003	44.6	0.013
Oil	35.2	0.03	41.4	0.051
S_1	31.7	0.06	38.5	0.071
Alcohol	29.2	0.005	35.4	0.055
S_2	25.4	0.02	33.8	0.15
S_3	16	0.09	26.8	0.058
S_4	13.9	0.14	26.5	0.033
Water	1	0.01	17.6	0.046

The mean phase values obtained from the RFID reader for the three pure materials along with the four sample mixtures are plotted against their relative permittivity values at 22 ºC and 40 ºC as shown in Fig. 5.8 (a) and (b), respectively. In both the cases, the first data point represent air (used as a reference) having ϵ_r = 1, and the last data point represent 100% water with ϵ_r= 79 at 22 ºC and ϵ_r= 73 at 40 ºC . Since the permittivity of the air as well as the three pure materials are known, the effective permittivity for the unknown samples can be determined using the linear curve fitting

equation obtained from the recorded phase values for both the lower and higher temperature measurements. In the Fig. 5.8, each mixture sample is denoted by a subscript S_n, where, n is the sample number.

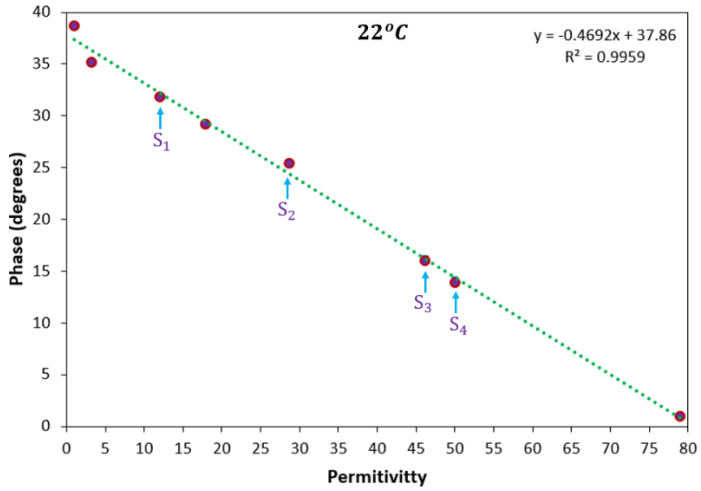

(a)

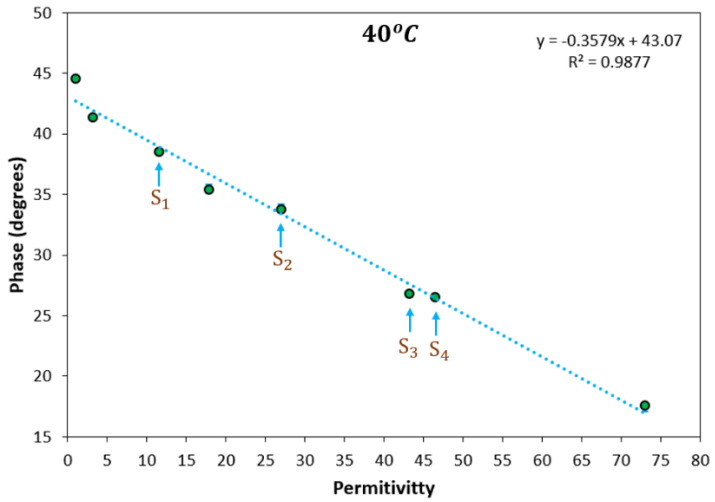

(b)

Figure 5.8: Phase with respect to permittivity for samples and pure materials at (a) 22 °C (b) 40 °C .

The sensitivity of the proposed material characterization sensor is calculated using the equation introduced in chapter 3. In this case the equation is modified as the ratio between the overall phase variation and the total change in the real permittivity value as given by 5-3.

$$S_{\frac{\delta\phi}{\delta\varepsilon}} = \left(\frac{\phi_1 - \phi_0}{\varepsilon_1 - \varepsilon_0}\right) \quad \text{…….. (5-3)}$$

Where, ϕ_0 is the phase value related to the lowest permittivity value ε_0 and ϕ_1 is the phase value related to the highest permittivity value ε_1.

Based on the above equation, the calculated sensitivity of the sensor is 0.47^{o} per 1 digit change in the real permittivity.

Since the same RFID reader was used similar to the sensing systems demonstrated in the previous chapters with a phase detection accuracy of about $\pm 1^{o}$, therefore, the resolution of the proposed sensor is calculated using the mathematical expression below.

$$Resolution = \frac{2^{\mathrm{o}}}{0.47^{\mathrm{o}}} = 4.2$$

The obtained resolution of the sensor confirm that the sensor can accurately detect a minimum variation of 4.2 in the real permittivity values.

5.2.1. Sensor Validation

The phase measurement results of the proposed passive wireless sensor are validated by repeating the experiments using a ROHDE & SCHWARZ Vector Network

Analyzer for all the samples at two temperatures as demonstrated in Fig. 5.9. Unlike the measurement setup explained in the previous section, the output of the sensor was recorded using VNA instead of the wireless RFID reader. All the samples from the previous measurements were utilized to keep the measurement consistency between the two proposed methods. An electromechanical mixer was used for constant agitation of the mixtures during the experiments. For each sample two phase measurements were taken at 22 ^{o}C and 40 ^{o}C , by utilizing the ceramic resistor as a heater and using a reference temperature sensor for monitoring the sample temperature during the tests. The comparison plots of Fig. 5.10 (a) and (b), shows that both the results obtained from the VNA measurements as well as the RFID reader are in good agreement. The small variation in the results is due to differences in the measurement setup, i.e. in case of the measurements taken with RFID reader, some extra components are required for wireless transmission of the sensor data from node to the reader. These results demonstrate that the phase variation caused by the sensing element due to the difference in the real permittivity profiles of each sample is accurately sent wirelessly to the RFID reader.

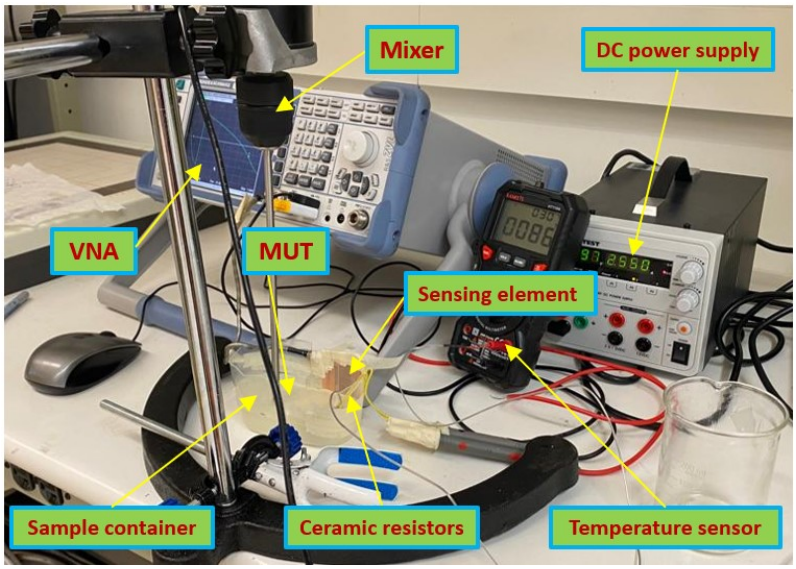

Fig. 5.9: Experimental setup for phase measurement with VNA.

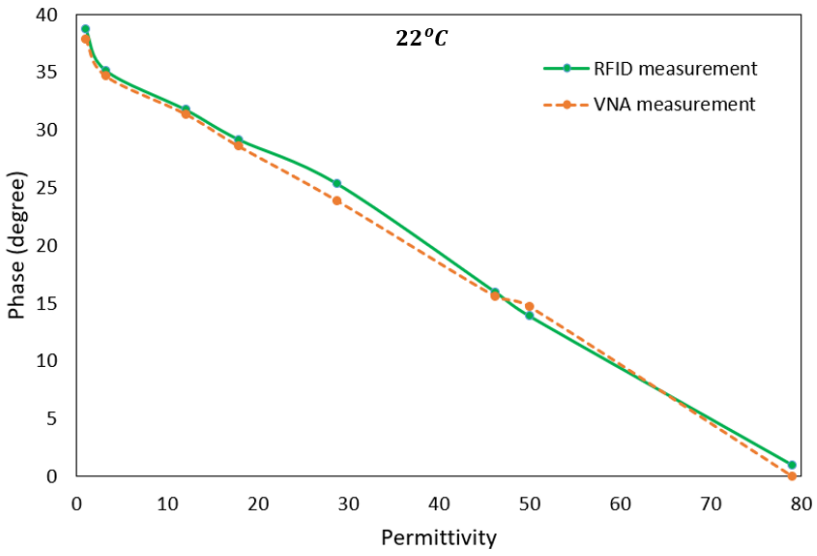

(a)

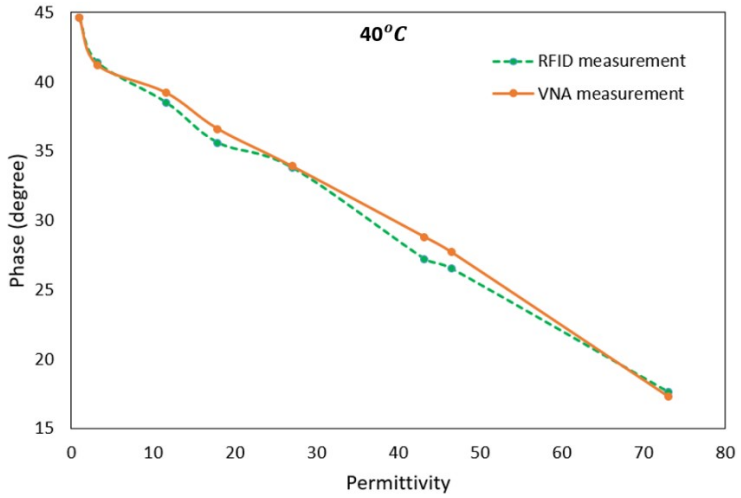

(b)

Fig. 5.10: Comparison of the phase values obtained from the RFID reader and VNA measurements at (a) 22 ºC (b) 40 ºC.

5.2.2. Volume Fraction Measurement

To verify the multivariable sensing capability of the sensor, the prepared samples with different component ratios were tested and numerically analyzed. The calculated sample volumetric fractions based on the proposed method is summarized and compared with the actual volume fraction of each sample represented in Table 5.2. Results show that the proposed sensor performs very well for calculating the volume fractions of a multivariable mixture. The accuracy of the sensing method is further quantified by calculating the mean absolute error (MAE) for all the samples as given in (5-4),

$$MAE = \frac{1}{n}\sum_{i=1}^{n}|z_i - x_i| \quad \text{.....} \quad (5\text{-}4)$$

Where, z_i is the actual volume fraction of each component used in sample preparation and x_i is the measured value based on the proposed method. From the results the maximum MAE is 4.6%, showing a better accuracy of the sensor for multivariable sensing. The cause of this error is mostly experimental error such as residue from previous sample measurement, as the same container was used to maintain the measurement consistency. Some additional causes such as sample preparation and difference in the viscosity of the samples can also add to the overall error in the volume concentrations. The proposed method wirelessly estimates the volume fractions of a mixture passively in real-time with a limited frequency bandwidth by utilizing multi-temperature measurements. Moreover, the method is expandable to multi-frequency multi-temperature sensing to detect more materials or to reduce the measurement error when a wider bandwidth is accessible. Based on its unique attributes, the presented sensor has a great potential to be commercially utilized for passive wireless estimation of volumetric concentration of multivariable mixtures in real-time.

TABLE 5.2: Comparison between the actual and calculated volume fractions of each sample mixture.

Volume fraction	100% Oil	100% Alcohol	Sample 1	Sample 2	Sample 3	Sample 4	100% Water
Actual Oil Volume(%)	100	0	80	50	10	30	0
Calculated Oil Volume(%)	97	0	84	57	9	33	0
Actual Alcohol Volume(%)	0	100	10	20	40	10	0
Calculated Alcohol Volume(%)	1	98	7	16	41	5	1
Actual Water Volume(%)	0	0	10	30	50	60	100
Calculated Water Volume(%)	2	2	9	27	50	62	99
Mean Absolute Error(%)	1.6	1.3	2.6	4.6	0.6	3.3	0.6

5.3. Summary

A novel sensing method is developed that can wirelessly estimate the volume fractions of a multivariable sample in real-time without utilizing any internal power source at the sensor node. The sensing element is powered by a backscattered signal received from the RFID reader for obtaining the sensing parameters. The operation principle is based on the difference in the real permittivity profile of each component and the unique effective permittivity of the sample mixtures due to the difference in mixing ratios. Upon loading the sensor with samples having different permittivity profiles, results in phase variation of the input signal. Additional phase information can be obtained by heating the samples in the vicinity of the sensing element up to 40 ^{o}C, due to the fact that the real permittivity of some components in a mixture changes with the temperature increase. Using the measured phase data and the calibration information for the components used in the preparation of the samples, the unknown volume concentration for each sample can be calculated. Volumetric analysis shows that the proposed method offers high accuracy with a maximum error in volume fractions as low as 7% and a maximum MAE of 4.6%. The presented sensing method could be a promising solution for wireless low-power, real-time volumetric analysis of multivariable mixtures especially in a widespread IoT-based environment.

Chapter 6 Conclusion and Future Work

6.1. Conclusion

The goal of this thesis was to develop new sensing methods for wireless detection of physical parameters by utilizing passive RFID technology to improve sensing reliability and power efficiency as well as to reduce design cost and complexity. Various types of capacitive sensing elements were designed and integrated with a power-less RFID sensing architecture, focusing on specific applications.

In chapter 3, an initial feasibility of the capacitive IDC based sensing element was evaluated. The sensing element was tested for moisture content detection in soil as well as air. Phase variation of the input signal with respect to change in the water content concentration of the MUT was used as a measuring parameter for sensing. The sensing element demonstrates highly sensitive and linear response to the moisture content variation of the test medium.

A new wireless sensing method for remote detection of the liquid level is proposed in chapter 4, by designing a capacitive sensing element and integrating it with a three-port UHF RFID sensing architecture. The variation in liquid level causes capacitance change in the sensing element that alters the phase of the input RFID backscattered signal with high sensitivity. The phase variation from the sensing node can be received by a wireless RFID reader to extract the information of the liquid level. The proposed RFID based wireless system is capable of providing real-time information about the liquid level with a linear response and excellent repeatability.

Finally, the benefits of the passive RFID sensing are applied to the estimation of the volume fractions of a mixture by designing a wireless material characterization system. The sensing method is capable of obtaining the volume fractions of a binary as well as a multivariable mixture containing three unknown components, by utilizing a limited RFID frequency bandwidth and multi-temperature measurements of the test samples. The sensor offers promising accuracy with a maximum mean absolute error of 4.6% in the calculated volume fractions of the unknown components in a multivariable mixture.

6.2. Future Work

This research work investigates the development of a new type of measurement methods for passive wireless sensing applications. Due to the importance of the topics related to the proposed concepts, this work can be extended to several other sensing applications as listed below:

- Wireless data sensing and monitoring in harsh environment with limited accessibility is an important area that needs to be further investigated. These applications require sensors that need less or almost no maintenance over time. The proposed sensing solutions are more reliable; however, the circuitry of the sensing nodes has to be modified to make it suitable for operation in a harsh environment such as extreme temperature, pressure, humidity etc. Since the designed measurement systems have the capability of wireless sensing, therefore, only the sensing nodes need to be modified.

- Due to the increase in the number of sensing devices, the future sensing applications focus on the data processing and control from several sensors at the same time to monitor multiple environmental parameters. Thus, further design investigation of the proposed sensing methods is necessary to include the capability of monitoring and data analysis received from multiple passive wireless sensors in real-time.
- The advancement in the IoT based sensing technologies requires new sensing techniques for the healthcare industry. Therefore, the current research directions can be extended to the development of non-invasive wearable healthcare products with the capability of low-power, low cost wireless detection and monitoring in a medical setting.

References

[1]. Ikpehai et al., “Low-power wide area network technologies for Internet-of-Things: A comparative review,” IEEE Internet Things J., vol. 6, no. 2, pp. 2225–2240, Apr. (2019).

[2]. J. Manyika, The Internet of Things: Mapping the Value Beyond the Hype, McKinsey Global Inst., Chicago, IL, USA, 2015. Accessed: Jul. 26, 2020.

[3]. R. Parada, J. Melia-Segui, M. Morenza-Cinos, A. Carreras, and R. Pous, “Using RFID to detect interactions in ambient assisted living environments,” IEEE Intell. Syst., vol. 30, no. 4, pp. 16–22, Jul./Aug. 2015.

[4]. S. Naderiparizi, A. N. Parks, Z. Kapetanovic, B. Ransford, and J. R. Smith, “WISPCam: A battery-free RFID camera,” in Proc. IEEE Int. Conf. RFID, 2015, pp. 166–173.

[5]. M. M. Honari, H. Saghlatoon, R. Mirzavand, and P. Mousavi, “An RFID sensor for early expiry detection of packaged foods,” in Proc. IEEE 18th Int. Symp. Antenna Technol. Appl. Electromagn. (ANTEM), 2018, pp. 1–2.

[6]. Archer, D. G. and P. Wang. “The Dielectric Constant of Water and Debye-Hückel Limiting Law Slopes," Journal of Physical and Chemical Reference Data 19, 371-411, (1990).

[7]. N. H. H. Abdullah., N. W. Kuan., A. Ibrahim., B. N. Ismail., M. R. A. Majid., R. Ramli., and N. S. Mansor. “Determination of soil water content using time domain reflectometer (TDR) for clayey soil," AIP Conference Proceedings, 020016, (2018).

[8]. K. Sarabandi., E.S. Li. “Characterization of soil moisture using a microstrip resonator," Geoscience and Remote Sensing Symposium, IGARSS ’94. ’Surface and Atmospheric Remote Sensing: Technologies, Data Analysis and Interpretation,, pp. 1445-1447, (1994).

[9]. A. Verma., N. K. Tiwari and M. J. Akhtar. “Soil moisture detection using CSRR based submersible RF sensor," 2018 3rd International Conference on Microwave and Photonics (ICMAP), pp. 1-2, (2018).

[10]. B. Gao., Z. Chen., X. Gong., P. Wang and L. Tong. “Design and Experiment of Microwave Soil Moisture Sensor," IGARSS 2020 - 2020 IEEE International Geoscience and Remote Sensing Symposium, pp. 5053-5056, (2020).

[11]. Pandey, Gunjan & Kumar, Ratnesh & Weber, Robert. “Determination of Soil Ionic Concentration using Impedance Spectroscopy," Proceedings of SPIE - The International Society for Optical Engineering, (2013).

[12]. Furqan CM., Khan MU., Awais M., Jiang F., Bae J., Hassan A., Kwok HS. “Humidity sensor based on Gallium Nitride for real time monitoring applications," Sci Rep, 27;11(1):11088, (2021).

[13]. Markevicius, Vytautas & Navikas, D. & Valinevicius, Algimantas & Andriukaitis, Darius & Cepenas, Mindaugas. “The Soil Moisture Content Determination Using Interdigital Sensor," Elektronika ir Elektrotechnika, 18. 25-28. 10.5755, (2012).

[14]. Harris, N.R & Stonard, Alexander. “A Printed Capacitance Sensor for Soil Moisture Measurement," Proceedings. 2. 705. 10.3390, (2018).

[15]. Paczesny, Daniel & Tarapata, Grzegorz & Marzecki, Michal & Jachowicz, Ryszard. “The Capacitive Sensor for Liquid Level Measurement Made with Ink-jet Printing Technology," Procedia Engineering. 120. 731-735. 10.1016, (2015).

[16]. Olthuis, W. et al. “Theoretical and experimental determination of cell constants of planar-interdigitated electrolyte conductivity sensors,” Sensors and Actuators B-chemical, 252-256 (1995).

[17]. Abu-Abed, Alaeddin & Lindquist, Robert. “Capacitive interdigital sensor with inhomogeneous nematic liquid crystal film," Progress in Electromagnetics Research B, 7. 75-87, (2008).

[18]. Won, Jonghwa & Choa, Sung-Hoon & Yulong, Zhao. “An integrated sensor for pressure, temperature, and relative humidity based on MEMS technology," Journal of Mechanical Science and Technology - J MECH SCI TECHNOL, 20. 505-512, (2006).

[19]. Li, Bintian & Xiao, Gang & Liu, Feng & Qiao, Yan & Li, Chang & Lu, Zhisong. “Flexible Humidity Sensor Based on Silk Fabric for Human Respiration Monitoring," Journal of Materials Chemistry C, (2018).

[20]. Blank, Tamara & Eksperiandova, Lyudmyla & Belikov, Konstantin. “Recent trends of ceramic humidity sensors development: A review," Sensors and Actuators B: Chemical, (2016).

[21]. Khan, Muhammad Umair & Awais, Muhammad & Chattha, Tahseen & Hassan, Arshad & Bae, Jinho. “All printed wide range humidity sensor array combining MoSe2 and PVOH in series," Journal of Materials Science: Materials in Electronics, (2020).

[22]. S. H. Woodside. “Fiber optic continuous liquid level sensor," U.S. Patent, 4,994,682, Feb. 19, (1991).

[23]. E. O. Doebelin and D. N. Manik. “Measurement Systems: Application and Design," 6th ed. New York, NY, USA: McGraw-Hill, pp.518–569, (2011).

[24]. Bera SC, Mandal H, Saha S, Dutta A. “Study of a modified capacitance type level transducer for any type of liquid," IEEE Trans Instrum Meas, 63(3):641–9, (2014).

[25]. Liu B, Wang DY, Wang A. “Liquid-surface-level sensing based on transverse pulse train technique," IEEE Sens, 16(8):2317–21, (2016).

[26]. O. B. Akan, O. Cetinkaya, C. Koca, and M. Ozger. “Internet of hybrid energy harvesting things," IEEE Internet ThingsJ. vol. 5, no.2, pp. 736–746, Apr. (2018).

[27]. toghyani rizi, Majid & Shahrokh Abadi, M.H. “Analytical modeling of a coaxial cylindrical probe capacitive sensor based on MATLAB/Simulink for conductive liquids level measurements," Turkish Journal of Electrical Engineering and Computer Sciences, (2017).

[28]. Hui-Xin Zhang, Yu-Long Hou, Li-Shuang Feng, Shan Su, Jia-Wei Zhang, Jia Liu, Wen-Yi Liu, Jun Liu and Ji-Jun Xiong. “Polymer Optical Fiber Continuous Liquid Level Sensor for Dynamic measurement," IEEE Sensors Journal, Vol.15, No. 9, pp.5238-5242, (2015).

[29]. T.Vontz and V.Magori. “An ultrasonic flow meter for industrial applications using a helical sound path," Proc. IEEE Symp.Ultrasonics, Vol.2, pp.1047–1050, (1996).

[30]. Karimi, Muhammad & Arsalan, Muhammad & Shamim, Atif. “A low cost, printed microwave based level sensor with integrated oscillator readout circuitry,” 2017 IEEE MTT-S International Microwave Symposium (IMS), pp. 1742-1745, (2017).

[31]. F. Lucklum and B. Jakoby. “Non-contact liquid level measurement with electromagnetic-acoustic resonator sensors," Measurement Science and Technology, vol. 20, no. 12, p. 124002, (2009).

[32]. S. F. Ali and N. Mandal. “Design and Development of an Electronic Level Transmitter Using Inter Digital Capacitor," IEEE Sensors Journal, vol. 19, no. 13, pp. 5179-5185, (2019).

[33]. C. -S. A. Gong, H. K. Chiu, L. R. Huang, C. H. Lin, Z. D. Hsu and P. -H. Tu. “Low-Cost Comb-Electrode Capacitive Sensing Device for Liquid-Level Measurement," IEEE Sensors Journal, vol. 16, no. 9, pp. 2896-2897, (2016).

[34]. A. Guillet, A. Vena, E. Perret and S. Tedjini. “Design of a chipless RFID sensor for water level detection," International Symposium on Antenna Technology and Applied Electromagnetics, pp. 1-4., (2012).

[35]. R. Bhattacharyya, C. Floerkemeier and S. Sarma. “RFID tag antenna based sensing: Does your beverage glass need a refill?," EEE International Conference on RFID, pp. 126-133., (2010).

[36]. Goncalves, Ricardo & Rima, Sergi & Magueta, Roberto & Pinho, Pedro & Collado, Ana & Georgiadis, Apostolos & Hester, Jimmy & Carvalho, Nuno & Tentzeris, Manos. “RFID-Based Wireless Passive Sensors Utilizing Cork Materials," EEE Sensors Journal, 15.1-1., (2015).

[37]. Swiefy, Bassant & Sadek, Hala & Ahmed, Mohamed & Anis, Wagdy.R. “ Novel Conformal RF Tag for Level Detection," EEE International Conference on RFID, 645-646. 10.1109/IEEECONF35879.2020.9329939., (2020).

[38]. Węglarski, M.; Jankowski-Mihułowicz, P. “Factors Affecting the Synthesis of Autonomous Sensors with RFID Interface," Sensors, 19, 4392., (2019). https://doi.org/10.3390/s19204392.

[39]. H. Solar, A. Beriain, A. Rezola, D. del Rio and R. Berenguer, “A 22-m Operation Range Semi-Passive UHF RFID Sensor Tag With Flexible Thermoelectric Energy Harvester," IEEE Sensors Journal, vol. 22, no. 20, pp. 19797-19808, 15 Oct.15, (2022), doi: 10.1109/JSEN.2022.3202634.

[40]. P. Kalansuriya, R. Bhattacharyya and S. Sarma, “A novel communication method for semi-passive RFID based sensors," IEEE International Conference on Communications (ICC), pp. 5902-5907, (2014). doi: 10.1109/ICC.2014.6884264.

[41]. J. Fernández-Salmerón, A. Rivadeneyra, F. Martínez-Martí, L. F. CapitánVallvey, A. J. Palma, and M. A. Carvajal, “Passive uhf rfid tag with multiple sensing capabilities," Sensors, vol. 15, no. 10, pp. 26 769–26 782, (2015).

[42]. R. Vyas, V. Lakafosis, H. Lee, G. Shaker, L. Yang, G. Orecchini, "Inkjet printed, self powered, wireless sensors for environmental, gas, and authentication-based sensing," IEEE Sensors Journal, vol. 11, no. 12, pp. 3139–3152, Dec 2011.

[43]. Khalid, Nabil & Mirzavand, Rashid & Saghlatoon, Hossein & Honari, Mohammad Mahdi & Mousavi, Pedram. ‘A Three-Port Zero-Power RFID Sensor Architecture for IoT Applications," IEEE Access, PP. 10.1109, IEEE Access, PP. 10.1109, (2020).

[44]. A. Mason, O. Korostynska, M. Ortoneda-Pedrola, A. Shaw, A. Al-Shamma’a, A resonant coplanar sensor at microwave frequencies for biomedical applications, Sens. Actuators A 202 (2013).

[45]. S. Kulkarni, M.S. Joshi, Design and analysis of shielded vertically stacked ring resonator as complex permittivity sensor for petroleum oils, IEEE Trans. Microw. Theory Tech. 63 (8) (2015).

[46]. M. Baghelani, N. Hosseini and M. Daneshmand, "Selective Measurement of Water Content in Multivariable Biofuel Using Microstrip Split Ring

Resonators," 2020 IEEE/MTT-S International Microwave Symposium (IMS), 2020, pp. 225-228, doi: 10.1109/IMS30576.2020.9223908.

[47]. S. Mohammadi, K.K. Adhikari, M.C. Jain, M.H. Zarifi, High-resolution, sensitivity- enhanced active resonator sensor using a substrate-embedded channel for characterizing low concentration liquid mixtures, IEEE Trans. Microw. Theory Tech. 70 (1) (2022) 573–586, https://doi.org/10.1109/TMTT.2021.3109599.

[48]. A.P. Gregory, R.N. Clarke, A review of RF and microwave techniques for dielectric measurement on polar liquids, IEEE Trans. Dielectr. Electr. Insul. 13 (4) (2006) 727–743, https://doi.org/10.1109/TDEI.2006.1667730.

[49]. J. Sorocki, I. Piekarz, K. Wincza, S. Gruszczynski, J. Papapolymerou, Broadband microwave microfluidic coupled-line sensor with 3-D-printed channel for industrial applications, IEEE Trans. Microw. Theory Tech. 68 (7) (2020) 2808–2822, https://doi.org/10.1109/TMTT.2020.2972525.

[50]. Silavwe, E., Somjit, N. & Robertson, I. D. A Microfluidic-Integrated SIW Lab-on-Substrate Sensor for Microliter Liquid Characterization. IEEE Sensors Journal 16, 7628–7635 (2016).

[51]. Aydinalp C, Joof S, Dilman I, Akduman I, Yilmaz T. Characterization of Open-Ended Coaxial Probe Sensing Depth with Respect to Aperture Size for Dielectric Property Measurement of Heterogeneous Tissues. Sensors. 2022; 22(3):760. https://doi.org/10.3390/s22030760.

[52]. Turgul, V. & Kale, I. Characterization of the Complex Permittivity of Glucose/Water Solutions for Noninvasive RF/Microwave Blood Glucose Sensing. IEEE International Instrumentation and Measurement Technology Conference Proceedings (I2MTC) 1–5 (2016).

[53]. Park, E.-Y., Baik, J., Kim, H., Park, S.-M. & Kim, C. Ultrasound-modulated optical glucose sensing using a 1645 nm laser. Sci. Rep. 10(1), 1–9 (2020).

[54]. Boyer, C., Duquenne, A.-M., & Wild, G. (2002). Measuring techniques in gas–liquid and gas– liquid–solid reactors. Chemical Engineering Science, 57(16), 3185–3215. https://doi.org/10.1016/S0009-2509(02)00193-8.

[55]. Powell, Robert L. "Experimental techniques for multiphase flows." Physics of fluids 20.4 (2008): 040605.

[56]. Rahman, O.; Islam, T.; Ahmad, A.; Parveen, S.; Khera, N.; Khan, S.A. Cross Capacitance Sensor for Insulation Oil Testing. IEEE Sens. J. 2021, 21, 20980–20989.

[57]. A. Wang, Q. Marashdeh, B. J. Motil, and L.-S. Fan, "Electrical capacitance volume tomography for imaging of pulsating flows in a trickle bed," Chemical Engineering Science, vol. 119, pp. 77 – 87, 2014.

[58]. Benini, L., Farella, E., Guiducci, C, "Wireless sensor networks: Enabling technology for ambient intelligence," Microelectron. J., 37, 1639-1649, 2006.

[59]. S. Caizzone, C. Occhiuzzi and G. Marrocco, "Multi-chip RFID antenna integrating shape-memory alloys for temperature sensing," Proceedings of the 5th European Conference on Antennas and Propagation (EUCAP), pp. 2810-2813, 2011.

[60]. Weglarski M, Jankowski, Mihulowicz P, Pitera G, Jurkow D, Dorczynski M, "LTCC Flow Sensor with RFID Interface," Sensors (Basel)., 2020 Jan 2;20(1):268, 2020. doi: 10.3390/s20010268. PMID: 31906575; PMCID: PMC6983026.

[61]. Rennane, A., Fonseca, N., Abdelnour, A., Benmahmoud, F., Kaddour, D., Touhami, R., Tedjini, S, "Passive UHF RFID Sensor Tag for Pressure and Temperature Conditions Monitoring," Proceedings of the 2nd URSI Atlantic Radio Science Meeting (AT-RASC), Meloneras, Spain, pp. 1-3, 28 May-1 June 2018.

[62]. R. A. Potyrailo, C. Surman, W. G. Morris, S. Go, Y. Lee, J. Cella and K. S. Chichak, "Selective quantitation of vapors and their mixtures using individual passive multivariable RFID sensors," 2010 IEEE International Conference on RFID (IEEE RFID), pp. 22-28, 2010.

[63]. M. A. Ennasar, M. Essaaidi, O. El Mrabet and M. El Khamlichi,"Concentration Measurements of Ethanol in Water Based on RFID-UHF Flexible Sensor for Sterilization Against SARS-CoV," Microwave Mediterranean Symposium (MMS), pp. 1-4, 2022. doi: 10.1109/MMS55062.2022.9825563.

[64]. Ennasar, Mohammed Ali & El Mrabet, Otman & Kanjaa, Mohammed & Essaaidi, Mohamed,“Design and Characterization of a Broadband Flexible Polyimide RFID Tag Sensor for NaCl and Sugar Detection,” Progress In Electromagnetics Research C.,Vol.94,. 273-283. 10.2528/PIERC19052402, 2019.

[65]. Mulloni, Viviana, Giada Marchi, Leandro Lorenzelli, and Massimo Donelli,“Chipless RFID Sensing System for Precise Ethanol Determination in Alcoholic Solutions,” Electronics,11, no. 5: 735. 2022. doi.org/10.3390/electronics11050735.

[66]. M. H. Zarifi and M. Daneshmand,“High-Resolution RFID Liquid Sensing Using a Chipless Tag,” IEEE Microwave and Wireless Components Letters,vol. 27, no. 3, pp. 311-313, March 2017, doi: 10.1109/LMWC.2017.2662321.

[67]. K. Brinker and R. Zoughi,“Embedded chipless RFID measurement methodology for microwave materials characterization,” IEEE International Instrumentation and Measurement Technology Conference (I2MTC), pp. 1-6, 2018. doi: 10.1109/I2MTC.2018.8409670.

[68]. R. Gonc¸alves et al.,”RFID-Based Wireless Passive Sensors Utilizing Cork Materials,” IEEE Sensors Journal, vol. 15, no. 12, pp. 7242-7251, Dec. 2015, doi: 10.1109/JSEN.2015.2472980.

[69]. Zhao, Aobo & Zhang,”IQ signal based RFID sensors for defect detection and characterisation,” Sensors and Actuators A: Physical, 269. 10.1016/j.sna.2017.11.008, 2017.

[70]. X. Qian, Z. Li, Z. Meng, N. Gao and Z. Zhang,”Flexible RFID Tag for Sensing the Total Minerals in Drinking Water via Smartphone Tapping,” IEEE Sensors Journal, vol. 21, no. 21, pp. 24749-24758, 1 Nov.1, 2021, doi: 10.1109/JSEN.2021.3113797.

[71]. Olthuis, W. et al. “Theoretical and experimental determination of cell constants of planar-interdigitated electrolyte conductivity sensors,” Sensors and Actuators B-chemical, 252-256 (1995).

[72]. Abu-Abed, Alaeddin & Lindquist, Robert. “Capacitive interdigital sensor with inhomogeneous nematic liquid crystal film," Progress in Electromagnetics Research B, 7. 75-87, (2008).

[73]. Vadim F. Lvovich., C.C. Liu., Matthew F. Smiechowski. “Optimization and fabrication of planar interdigitated impedance sensors for highly resistive non-aqueous industrial fluids," Sensors and Actuators B: Chemical, Volume 119, Issue 2, (2006).

[74]. Kim, Chon-ung & Li, Guofeng & Li, Jie & Jong, Hakchol & Ro, Cholwu & Song, Yunho & Pak, Gilhung & Im, Songil. “Numerical analysis on effective electric field penetration depth for interdigital impedance sensor," Journal of Physics Conference Series. 418. 2020- .10.1088/1742-6596/418/1/012020, (2013).

[75]. Hammarling, Krister & Engholm, Magnus & Andersson, Henrik & Sandberg, Mats & Nilsson, Hans-Erik. “Broad-Range Hydrogel-Based pH Sensor with Capacitive Readout Manufactured on a Flexible Substrate," Chemosensors. 6. 30. 10.3390/chemosensors6030030, (2018).

[76]. Luo, Bing & Wang, Tingting & Zhang, Fuzeng & Lin, Yibin & Zheng, Chaozhi & Chen, She. “Interdigital Capacitive Sensor for Cable Insulation Defect Detection: Three-Dimensional Modeling, Design, and Experimental Test," Journal of Sensors, (2021).

[77]. Dean, Robert & Rane, Aditi & Baginski, Michael & Richard, Jonathan & Hartzog, Zane & Elton, David. “A Capacitive Fringing Field Sensor Design for Moisture Measurement Based on Printed Circuit Board Technology," Instrumentation and Measurement, IEEE Transactions on. 61. 1105-1112. 10.1109/TIM.2011.2173041, (2012).

[78]. Khan, Muhammad Umair & Hassan, Gul & Shaukat, Rayyan & Chougale, Mahesh & Kim, Jungmin & Bae, Jinho. “Wide range and highly linear signal processed systematic humidity sensor array using Methylene Blue and Graphene composite," Scientific Reports. 11. 10.1038/s41598-021-95977-6, (2021).

[79]. Islam, Tarikul & Mittal, Upendra & Nimal, A.T. & Sharma, M.U. “A nanoporous thin-film miniature interdigitated capacitive impedance sensor for

measuring humidity," International Journal of Smart and Nano Materials. 5. 169-179. 10.1080/19475411.2014.935833, (2014).

[80]. Kim, Ji-Hong & Moon, Byung-Moo & Hong, Sung-Min. "Capacitive Humidity Sensors Based on a Newly Designed Interdigitated Electrode Structure," Microsystem Technologies. 18. 10.1007/s00542-011-1373-0, (2012).

[81]. Nag, A., Mukhopadhyay, S.C., Kosel, J. Interdigitated Sensing and Electrochemical Impedance Spectroscopy. In: Printed Flexible Sensors. Smart Sensors, Measurement and Instrumentation, vol 33. Springer, Cham (2019).

[82]. Wang, D. et al. "Humidity sensor based on Ga2O3 nanorods doped with Na+ and K+ from GaN powder," Ceram. Int. 41, 14790– 14797. https://doi.org/10.1016/j.ceramint.2015.07.211, (2015).

[83]. Wang, C. et al. "A ZnO/porous GaN heterojunction and its application as a humidity sensor," Nanoscale Adv. 1, 1232–1239. https:// doi.org/10.1039/C8NA00243F, (2019).

[84]. Tsai, T.-Y. et al. "β-Ga2O3 Nanowires-based humidity sensors prepared on GaN/sapphire substrate," IEEE Sens. J. 13, 4891–4896. https://doi.org/10.1109/JSEN.2013.2274872, (2013).

[85]. Khalid, Nabil & Mirzavand, Rashid & Saghlatoon, Hossein & Honari, Mohammad Mahdi & Mousavi, Pedram. 'Three-Port Zero-Power RFID Flood Sensor for IoT Applications," IEEE Wireless Power Transfer Conference (WPTC), pp. 61-64, doi: 10.1109/WPTC48563.2020.9295554, (2020).

[86]. Chetpattananondh, Kanadit & Tapoanoi, T. & Phukpattaranont, P. & Jindapetch, Nattha. "A self-calibration water level measurement using an interdigital capacitive sensor," Sensors and Actuators A: Physical, 209. 175–182. 10.1016/j.sna.2014.01.040, (2014).

[87]. Mamishev, Alexander & Sundara-Rajan, Kishore & Yang, Fumin & Du, Yanqing & Zahn, Markus. "Determination of Soil Ionic Concentration using Impedance Spectroscopy," Interdigital sensors and transducers. Proceedings of the IEEE, (2004).

[88]. S. F. Ali and N. Mandal. “Design and Development of an Electronic Level Transmitter Using Inter Digital Capacitor," IEEE Sensors Journal, vol. 19, no. 13, pp. 5179-5185, (2019).

[89]. Rahman MZU, Aldossary OM, Islam T. “A constant phase impedance sensor for measuring conducting liquid level," ISA Trans. 2021, Sep;115:250-258, (2021).

[90]. F. A. Khan, A. Yousaf and L. M. Reindl. “Build-up detection and level monitoring by using capacitive glocal technique," 2016 European Frequency and Time Forum (EFTF), pp. 1-4, (2016).

[91]. K. R. Sandra, B. George and V. J. Kumar. “A Nonintrusive Magnetically Coupled Sensor for Measuring Liquid Level," IEEE Transactions on Instrumentation and Measurement, vol. 69, no. 10, pp. 7716-7724, Oct. (2020).

[92]. Lata, Anamika & Kumar, Brajesh & Mandal, Nirupama. “Design and development of a level transmitter using force resistive sensor as a primary sensing element," IET Science, Measurement and Technology, 12. 10.1049/iet-smt.2016.0513, (2017).

[93]. P. H. Dietz, D. Leigh and W. S. Yerazunis,. “Wireless liquid level sensing for restaurant applications," SENSORS, 2002 IEEE, pp. 715-720 vol.1, (2002).

[94]. Jin, Baoquan & Zhang, Zeyu & Zhang, Hongjuan. “Structure design and performance analysis of a coaxial cylindrical capacitive sensor for liquid-level measurement," Sensors and Actuators A: Physical. 223. 10.1016/j.sna.2014.12.027, (2015).

[95]. Musa, N., Onimisi, M. Y. & Ikyumbur, J. T, “Frequency and temperature dependence of ethanol using the Cole-Cole relaxation model”, Am. J. Condens. Matter Phys., 10(2), 44-49 2020.

[96]. N. Y. Onimisi and J. T. Ikyumbur, “Comparative analysis of dielectric constant and loss factor of pure butan-1-ol and ethanol”, Amer. J. Conden. Condens. Matter Phys., vol. 5, no. 3, pp. 69-75, 2015.

[97]. Andryieuski, A., Kuznetsova, S., Zhukovsky, S. et al., “Water: Promising Opportunities For Tunable All-dielectric Electromagnetic Metamaterials”, Sci Rep 5,13535, 2015. https://doi.org/10.1038/srep13535.